JACS
JOURNAL OF THE AMERICAN CHEMICAL SOCIETY
pubs.acs.org/JACS
Article

Development, Application, and Mechanistic Interrogation of a Dual Ni Catalysis Approach to Photoredox-Based C(sp^3)–C(sp^3) Cross-Coupling

Erin M. Bucci,[§] Melecio A. Perea,[§] Remy F. Lalisse, Poulami Mukherjee, T. Judah Raab, Lakshmy Kannadi Valloli, Daniel S. Min, Matthew J. Bird,* Osvaldo Gutierrez,* and Abigail G. Doyle*

Cite This: https://doi.org/10.1021/jacs.5c10906
Read Online

ABSTRACT: The installation of alkyl substituents such as methyl groups is a crucial tactic for the synthesis and diversification of medicinal compounds with improved pharmacological profiles. However, strategies that leverage methyl radical for C(sp^3) methylation remain underdeveloped due to the challenge of obtaining cross-selectivity between fleeting aliphatic radicals and alkyl electrophiles. We report the development, application, and interrogation of a conceptually novel mechanistic framework for C(sp^3)–Me bond formation using two distinct Ni catalysts capable of cross-coupling sterically and electronically diverse alkyl halides (chlorides and bromides) with methyl radical generated photocatalytically from benzaldehyde dimethyl acetal. Furthermore, by modifying the alkyl substituents on the acetal coupling partner, we demonstrate cross-couplings beyond methylation to access an array of 1°–1° and 1°–2° alkyl–alkyl bonds. Experimental and computational mechanistic studies provide support for cooperativity between an in situ-generated (bpy)Ni^{I}(X) catalyst that facilitates XAT and inner-sphere C–C bond formation and a (Tp*)Ni^{II}(acac) cocatalyst that captures methyl radical and engages in concurrent outer-sphere S_H2 coupling.

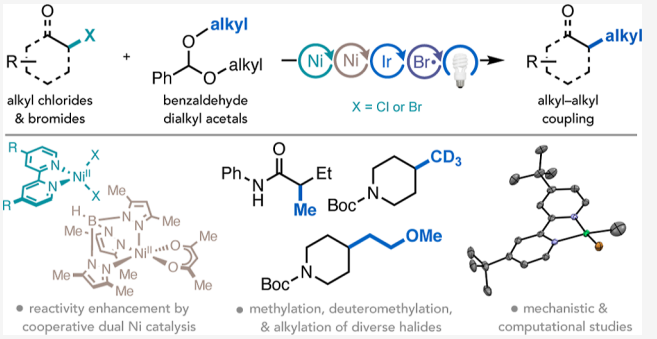

INTRODUCTION

The construction of C(sp^3)–C bonds by cross-coupling is a highly desirable reaction in medicinal chemistry for its potential to enable access to libraries of lead candidates with greater C(sp^3) character.[1−3] Ni catalysis under reductive,[4,5] photocatalytic,[6] or electrocatalytic[7,8] conditions has provided numerous solutions to this challenge by enabling the use of diverse aliphatic radical precursors for C(sp^3)–C(sp^2) and C(sp^3)–C(sp^3) cross-coupling. Along these lines, one of the key goals of Ni-catalyzed cross-coupling is to identify new combinations of fragments that can be linked together to access products occupying novel chemical space. Our group has a longstanding interest in addressing this goal by developing new reductive and photocatalytic Ni-catalyzed cross-couplings using unconventional electrophiles like acetals,[9−13] aziridines,[10,14−17] and epoxides[18−20] (Figure 1A). Acetals are of particular interest, owing to their wide availability and facile synthesis from abundant feedstock alcohols, as well as their diverse reactivity under catalytic Ni regimes.[9−13] For example, we recently found that commercially available benzaldehyde dimethyl acetal (**A1**, Figure 1B) can undergo bromine radical-mediated hydrogen atom transfer (HAT)/β-scission to generate methyl radical that can be coupled to either aryl halides[12,13] or aziridines.[10] The ring-opening aziridine methylation was particularly notable, as radical methylation at C(sp^3) centers can pose significant cross-selectivity challenges due to slow activation of alkyl electrophiles by Ni and promiscuous reactivity of the highly reactive methyl radical. While this work was crucial in demonstrating the HAT/β-scission strategy for C(sp^3) radical methylation, the aziridine substrates used for cross-coupling had a high degree of structural specificity, which, in turn, resulted in highly specific β-methylated amine products with an overall low degree of structural diversity. As a result, we questioned whether more generalizable substrates, such as alkyl halides, could be used instead to broadly expand the chemical space coverage of products accessible by this strategy (Figure 1C). Accordingly, we set out to develop a Ni/photoredox-catalyzed cross-coupling between diverse alkyl halides (chlorides and bromides) and methyl radical derived from

Received: June 27, 2025
Revised: October 24, 2025
Accepted: October 27, 2025

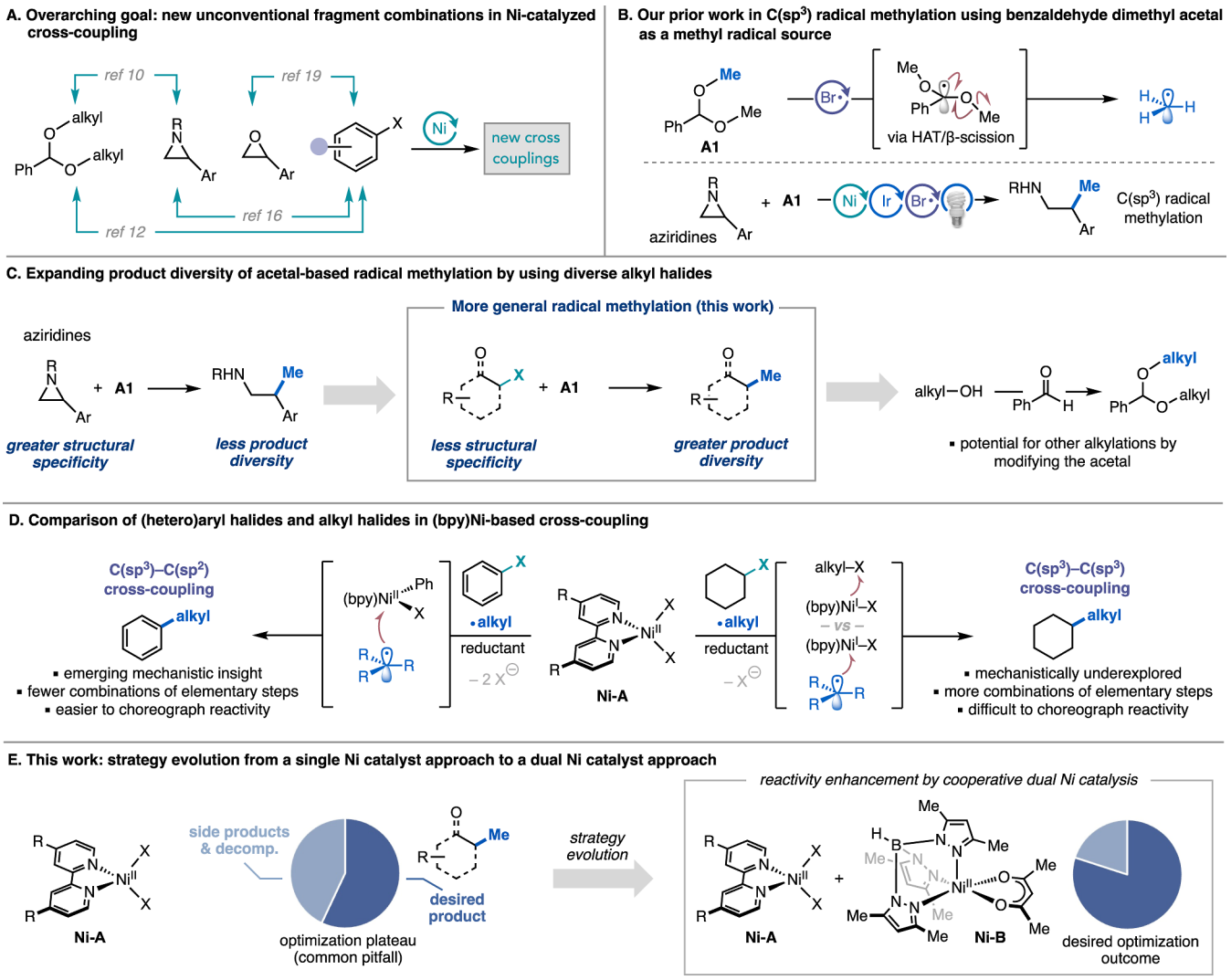

Figure 1. Background and strategy. (A) Overview of unconventional cross-electrophile coupling. (B) Our previous study of $C(sp^3)$ radical methylation of styrenyl aziridines using benzaldehyde dimethyl acetal as a methyl radical source. (C) Proposed extension of Ni/photoredox-catalyzed radical methylation to diverse alkyl halides. (D) Comparison of (bpy)Ni-based $C(sp^3)–C(sp^2)$ and $C(sp^3)–C(sp^3)$ cross-coupling using Ni/photoredox catalysis. (E) Strategy evolution from a single Ni catalyst approach to a cooperative dual Ni catalytic system, which enhances methylation and enables a general strategy for cross-coupling methyl radical to alkyl chlorides and alkyl bromides. Ar, aryl; Bpy, bipyridine; Ph, phenyl; X, halogen; HAT, hydrogen atom transfer; decomp., decomposition.

A1. Furthermore, we envisioned that this approach may extend to other alkylations by simply modifying the precursor alcohol used for benzaldehyde dialkyl acetal synthesis.

Despite the practical advantages of employing alkyl halides directly in radical-based methylation and alkylation, the inherent reactivity differences between alkyl and aryl halides present significant challenges in extending reaction conditions developed for $C(sp^2)–C(sp^3)$ cross-coupling to $C(sp^3)–C(sp^3)$ cross-coupling. Bipyridine (bpy) nickel complexes (e.g., **Ni–A**)[21] are often the catalyst of choice for cross-electrophile couplings with (hetero)aryl halides owing to their ability to activate aryl electrophiles via oxidative addition,[22−24] capture alkyl radicals,[25−27] and engage in $C(sp^3)–C$ reductive elimination.[28] Compared to radical-based $C(sp^3)–C(sp^2)$ cross-couplings with (hetero)aryl halides, (bpy)Ni-catalyzed $C(sp^3)–C(sp^3)$ cross-couplings with alkyl halides remain underexplored and entail choreographing the competitive elementary steps of radical capture and radical generation via halogen atom transfer (XAT)[29−31] at highly reactive (bpy)-$Ni^I(X)$ centers (Figure 1D). Specifically, using (bpy)Ni for both generating and capturing alkyl radicals ultimately makes it difficult to separately tune reactivity and achieve cross-selective coupling. For these reasons, most examples of Ni/photoredox-catalyzed $C(sp^3)–C(sp^3)$ radical coupling reactions rely on distinct Ni frameworks (e.g., $(Tp^*)Ni^{II}(acac)$), featuring a scorpionate-type ligand, such as tris(3,5-dimethyl-1-pyrazolyl)-borate (Tp^*), and a diketonate-type ligand, such as acetylacetonate (acac). These catalysts are generally biased toward specific mechanisms, like S_H2 coupling via radical sorting, which promote desired reactivity and cross-selectivity.[32−34]

https://doi.org/10.1021/jacs.5c10906
J. Am. Chem. Soc. XXXX, XXX, XXX−XXX

While effective for radical capture and C−C bond formation, this type of catalyst framework is not well-suited for XAT, thus rendering alkyl halide activation difficult. Given these mechanistic complexities, we sought to identify a Ni-catalyst framework that would be suitable for facilitating the desired radical-based methylation of C(sp^3)−halides with high yield and cross-selectivity.

Herein, we describe our realization of this goal following a two-stage evolution from a "single Ni catalyst" approach to a "dual Ni catalyst" approach (Figure 1E). By simultaneously evaluating mechanistic hypotheses and optimizing reaction conditions, we identified a potential divergence of the Ni precatalyst to two active species with orthogonal roles, thus leading us to shift optimization efforts toward strategically designing a dual Ni catalyst system that ultimately enabled significant reactivity enhancement. This article details efforts toward the development, application, and mechanistic interrogation of this strategy, which hinges upon a (bpy)Ni^{I}(X) catalyst (formed via reduction of **Ni−A**) working in concert with a (Tp*)Ni^{II}(acac) catalyst (**Ni−B**) to facilitate diverse alkyl halide methylation. While catalytic cooperativity between identical transition metals has shown great potential for enabling challenging C(sp^3)−C(sp^2) couplings,[35−37] such strategies in general remain underexplored and to the best of our knowledge have never been applied to alkyl−alkyl cross-coupling. Therefore, in addition to establishing a general strategy for alkyl halide methylation, we envision that this catalytic approach will also inspire and help facilitate the development of other selective C(sp^3)−C(sp^3) cross-coupling reactions.

RESULTS AND DISCUSSION

Reaction Development and Scope Evaluation. We commenced optimization studies by evaluating the cross-coupling of α-bromoamide **Br-1a** with a methyl radical derived from benzaldehyde dimethyl acetal (**A1**) to afford cross-coupled product **1b** (Figure 2A). Using 1 mol % Ir[dF(CF_3)-ppy]$_2$(dtbbpy)PF_6 as a photocatalyst, 2 mol % $NiBr_2$•glyme as a Ni precatalyst, 3 mol % dtbbpy as a ligand, and one equivalent of potassium phosphate as a base, under blue light irradiation, the desired cross-coupled product **1b** was observed in trace yields after 24 h along with a significant amount (65%) of protodehalogenated side product **1c** and nonspecific decomposition (entry 1). We hypothesized that **1c** may be forming via direct photocatalytic reduction of substrate **Br-1a** by the Ir photocatalyst. To probe this hypothesis, we performed a control study excluding Ni and ligand (entry 2) which resulted in comparable levels of **1c**, thus providing support for the reduction of **Br-1a** by Ir. To circumvent this undesired reduction and increase the ratio of **1b** to **1c**, the photocatalyst loading was decreased to 0.1 mol %; however, this modification led to a similar distribution of observed products with full consumption of the precursor bromide **Br-1a** (entry 3). With photocatalytic reduction of **Br-1a** proving to be a formidable challenge, we hypothesized that a structurally similar α-chloroamide (i.e., **Cl-1a**, Figure 2A) may be less prone to photocatalytic reduction due to the relatively stronger C−Cl bond and, thus, may help mitigate the formation of **1c** and increase the formation of the desired cross-coupled product (**1b**). This hypothesis was supported by cyclic voltammetry studies (see Supporting Information Figures S4 and S5) which revealed **Cl-1a** to have a higher reduction potential (E_{red} = − 2.29 V vs SCE in MeCN)

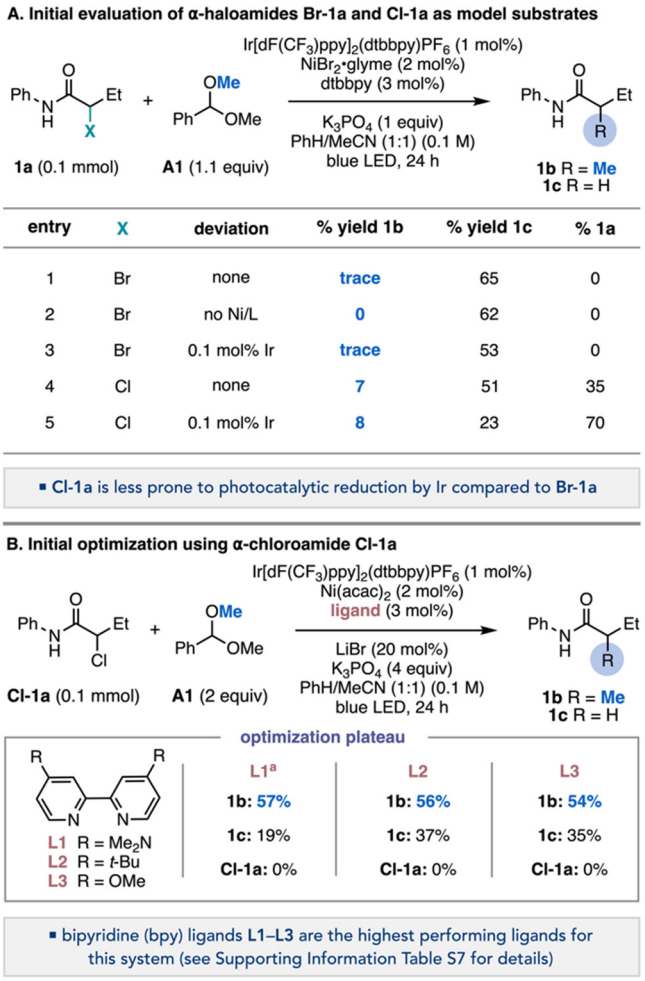

Figure 2. (A) Initial screening of the C(sp^3)−halide methylation using α-bromoamide **Br-1a** and α-chloroamide **Cl-1a**. (B) Optimization of the C(sp^3)−halide methylation using α-chloroamide **Cl-1a**. All yields determined by ^{1}H NMR or GC-FID analysis using 1,3,5-trimethoxybenzene as an external standard. [a]2 mol % ligand.

compared to **Br-1a** (E_{red} = − 1.85 V vs SCE in MeCN). Indeed, when the analogous set of experiments were performed using **Cl-1a**, we observed slightly increased formation of **1b** (7% yield, entry 4) at 1 mol % Ir loading along with decreased formation of **1c** (51% yield) and overall lower conversion of **Cl-1a** (35% recovered) to undesired side products. Unlike **Br-1a**, decreasing the Ir photocatalyst from 1 to 0.1 mol % led to a significant decrease in protodehalogenation (23% yield **1c**) and unproductive **Cl-1a** consumption (70% recovered), while maintaining desired product formation at 8% yield (entry 5). Further optimization efforts using α-chloroamide **Cl-1a** revealed that 2 mol % Ni(acac)$_2$ with an electron rich bpy ligand (2−3 mol % **L1**, **L2**, or **L3**) under photocatalytic conditions and in the presence of 20 mol % LiBr could deliver product in significantly improved quantities ranging from 54−57% yield (Figure 2B). In general, couplings with **L1** proceeded with less protodehalogenation (19%) compared to couplings using **L2** (36%) or **L3** (35%); however, further attempts to increase the yield of desired product in couplings using **L1**, **L2**, or **L3** by varying reaction parameters like Ni precatalyst/ligand identity and catalyst/reagent stoichiometry ultimately proved ineffective (see Supporting Information Section 3 for details).

https://doi.org/10.1021/jacs.5c10906
J. Am. Chem. Soc. XXXX, XXX, XXX−XXX

To overcome this plateau in yield, we sought to gain initial insight into the potential mechanistic scenarios governing reactivity that could help guide further optimization and improve reaction outcomes. As such, we began by reexamining how the identity of Ni precatalyst under the initial "standard" conditions influenced the yield and selectivity of the reaction. We found that diketonate-based Ni complexes (e.g., $Ni(acac)_2$ and $Ni(TMHD)_2$) performed significantly better than other Ni precatalysts, delivering product in 56% and 46% yield, respectively (Figure 3A). Given the effectiveness of such Ni-

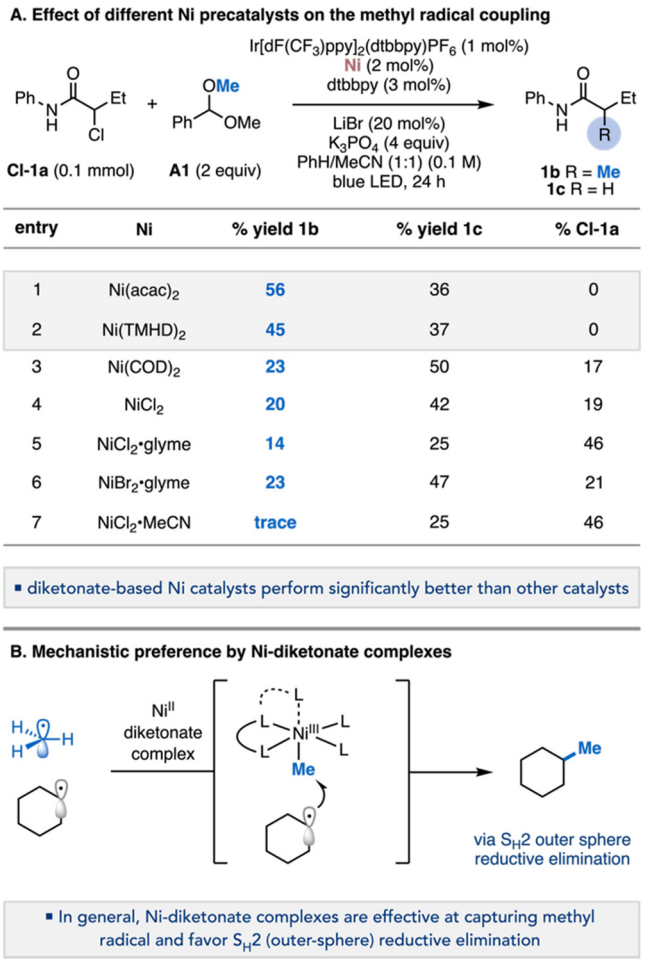

Figure 3. Significance of Ni-diketonate complexes on reaction outcome and possible mechanistic implications. All yields determined by GC-FID analysis using 1,3,5-trimethoxybenzene as an external standard.

diketonate catalysts at facilitating methyl radical capture, radical stabilization, and outer-sphere (i.e., S_H2) reductive elimination (Figure 3B), we hypothesized that these particular elementary steps may be pertinent to the reaction mechanism of the cross-coupling.[32−34] As such, we envisioned that a single (4,4′-R-bpy)Ni^I(acac) catalyst may be facilitating XAT activation of the alkyl halide, methyl radical capture, and outer-sphere C−C bond formation to forge the methylated product (Figure 4A). In this case, either inefficient Me radical capture or inefficient S_H2 at (bpy)Ni^{III}(acac)(Cl)(Me) could result in the observed formation of protodehalogenated side product **1c** due to the XAT-generated alkyl radical engaging in off-cycle HAT. Given the complex nature of Ni speciation in solution and the propensity for multiple active Ni species to be

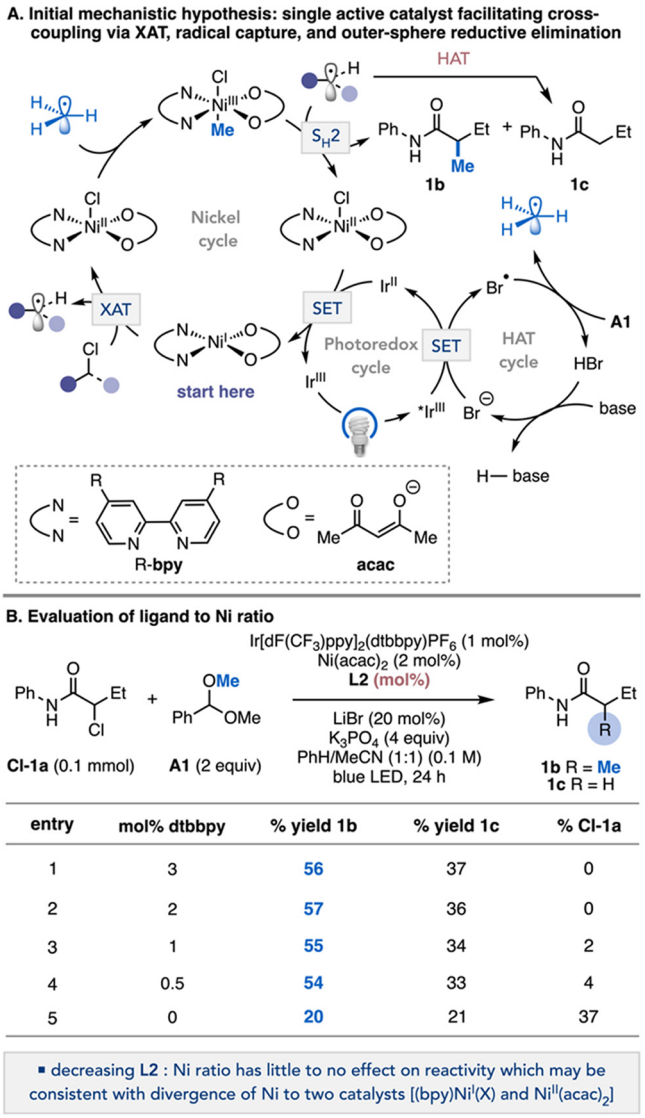

Figure 4. (A) Initial mechanistic hypothesis and (B) interrogation of single nickel system by evaluating the effect of ligand/Ni ratio on reaction outcome. All yields determined by GC-FID analysis using 1,3,5-trimethoxybenzene as an external standard.

present in catalytic reactions,[38] we performed a series of experiments varying the ligand to Ni ratio in the reaction to gain insight into the potentially active catalytic species present (Figure 4B). We hypothesized that if one active Ni species (i.e., (bpy)Ni^I(acac)) facilitates alkyl halide activation, methyl radical capture, and reductive elimination, then the yield of the reaction should be negatively impacted by decreasing the ratio of ligand to Ni. Interestingly, we observed that decreasing the ratio of **L2**:Ni from 1.5:1 to 0.25:1 had little to no effect on the yield of the reaction, formation of side product **1c**, or consumption of **Cl-1a** (Figure 4B, entries 1−4). However, when **L2** was excluded from the reaction entirely, the product yield, the formation of **1c**, and the consumption of **Cl-1a** all decreased (entry 5). These results suggested to us that while inclusion of a bpy ligand is important for desired reactivity, presumably due to its role in facilitating activation of **Cl-1a** via XAT by (bpy)Ni^I(acac),[31] unligated $Ni(acac)_2$ may also play an important role in the reaction mechanism.

https://doi.org/10.1021/jacs.5c10906
J. Am. Chem. Soc. XXXX, XXX, XXX−XXX

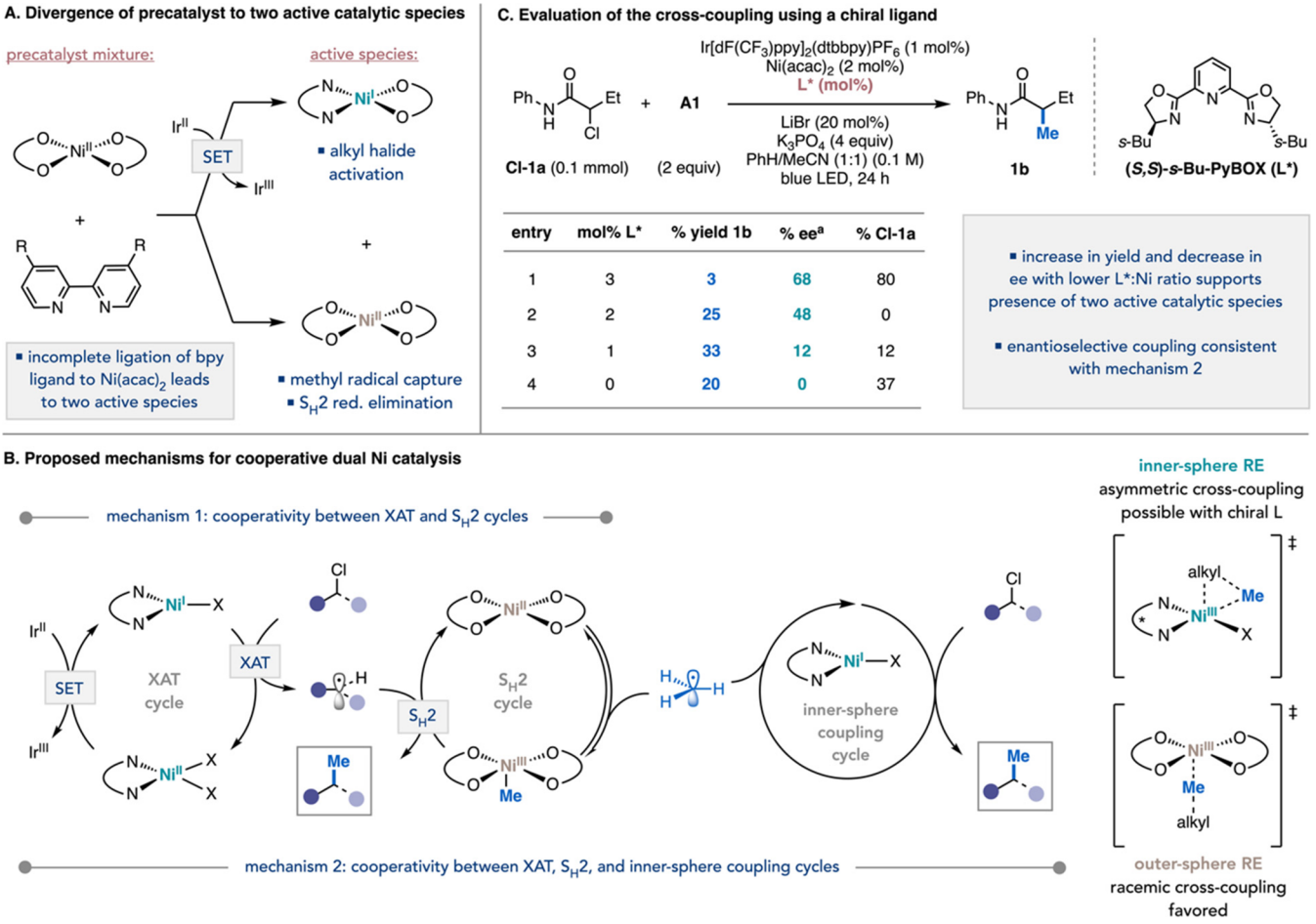

Figure 5. (A) Hypothesized divergence of the $Ni(acac)_2$ precatalyst to two active catalytic species following ligation with a bpy ligand and reduction by Ir^{II}. (B) Proposed mechanisms for cooperative dual Ni catalytic frameworks. (C) Assessing asymmetric cross-coupling with potential background outer-sphere reductive elimination. All yields determined by GC-FID analysis using 1,3,5-trimethoxybenzene as an external standard. [a]All enantiomeric excess (ee) values determined by chiral SFC analysis (see Supporting Information Section 3 for details).

Given these results, we postulated that perhaps the $Ni(acac)_2$ precatalyst forms two potentially active catalytic species in the presence of a bpy ligand and photocatalyst: $(bpy)Ni^{I}(acac)$, which may play a role in activating the alkyl chloride via XAT, and unligated $Ni^{II}(acac)_2$, which may be important for steps like methyl radical capture and S_H2 (i.e., outer-sphere) reductive elimination (Figure 5A). On the basis of this hypothesis, we shifted our attention to mechanistic proposals centered around two cooperative Ni catalysts (Figure 5B). Specifically, we envisioned two potential catalytic frameworks in which there is cooperativity either between XAT and S_H2 cycles (mechanistic proposal 1) or between XAT, S_H2, and inner-sphere coupling cycles (mechanistic proposal 2). For proposal 1, the $(bpy)Ni^{I}(X)$ catalyst (where X = acac, Cl, or Br) would serve to activate the alkyl halide via XAT,[31] while the unligated $Ni^{II}(acac)_2$ catalyst would capture acetal-derived methyl radical to generate $Ni^{III}(acac)_2(Me)$ free to engage in S_H2 coupling with the XAT-derived alkyl radical to produce **1b**. For proposal 2, these XAT and S_H2 cycles would still be operative but would function cooperatively with a second equivalent of $(bpy)Ni^{I}(X)$ catalyst facilitating concurrent cross-coupling via elementary steps commonly associated with inner-sphere cross-coupling (i.e., methyl radical capture, oxidative addition via XAT/radical rebound, and inner-sphere reductive elimination). Of note, given previous reports of employing Ni^{II} diketonate complexes as catalysts for outer-sphere C−C bond formation between two alkyl radical fragments,[32−34] these proposals would both be in line with the high performance of diketonate Ni precatalysts observed during optimization (Figure 3A). Similar to our initial mechanistic hypothesis, we next sought to interrogate the feasibility of these cooperative dual Ni catalysis proposals and distinguish between mechanisms 1 and 2. Specifically, we hypothesized that if mechanism 1 was operative, replacement of the bipyridine ligand at the XAT catalyst with a chiral ligand should still result in racemic cross-coupling since C−C bond formation would be occurring exclusively at the achiral $Ni^{III}(acac)_2(Me)$ center, via outer-sphere reductive elimination, and without influence from the chiral $(L^*)Ni^{I}(X)$ cocatalyst which in this case would only be facilitating XAT. However, if mechanism 2 was operative, then some enantioinduction should be feasible due to concurrent inner-sphere cross-coupling by $(L^*)Ni^{I}(X)$. As such, we investigated how the enantioselectivity of the methylation reaction is impacted by changing the ratio of a chiral ligand (**L***) to Ni. For these studies, we identified *s*-Bu-PyBOX (**L***) as a suitable ligand due to it providing modest levels of enantioinduction (Figure 5C). We found that at a ratio of 1.5:1 **L***:Ni, the reaction delivered product **1b** in 3% yield and 68% ee, with overall low conversion of **Cl-1a** (entry 1). In general,

https://doi.org/10.1021/jacs.5c10906
J. Am. Chem. Soc. XXXX, XXX, XXX−XXX

decreasing the ratio of **L***:Ni resulted in a higher yield of **1b** and higher conversion of **Cl-1a**, but with a corresponding decrease in enantiomeric excess (entries 2 and 3). Furthermore, when **L*** was excluded from the reaction completely, we observed a 20% yield of racemic **1b** (entry 4). The observed increase in yield and decrease in ee when lowering the **L***:Ni ratio correlated with a greater concentration of achiral $Ni^{II}(acac)_2$ being present in solution to facilitate racemic outer-sphere C−C bond formation. However, the observed enantioinduction in the presence of **L*** suggested that inner-sphere C−C bond formation may be operative from the Ni catalyst bearing an L-type nitrogen ligand (i.e., **L***, **L1**, **L2**, and **L3**). In a preliminary sense, these results were consistent with mechanistic proposal 2 (Figure 5B), in which C−C bond formation occurs via both an outer-sphere pathway (facilitated by $Ni^{II}(acac)_2$) and an inner-sphere pathway (facilitated by $(bpy)Ni^{I}(X)$). Overall, in the case of this mechanistic proposal, methyl radical capture at two distinct Ni complexes ($Ni^{II}(acac)_2$ and $(bpy)Ni^{I}(X)$) would enhance reactivity and cross-selectivity by more efficiently funneling excess reactive free methyl radical to the product via two complementary C−C bond forming pathways. While a major focus of later mechanistic studies (vide infra) would be to more accurately discern the sequence of elementary steps for the inner-sphere coupling process, we envisioned leveraging the core feature of this proposal, cooperativity between two Ni catalysts, to guide further reaction optimization.

With preliminary data suggesting a dual Ni catalytic regime, we decided to strategically design two catalysts (Figure 6A) that would be effective at the specific roles postulated to be mechanistically relevant if either mechanism 1 or 2 were operative (i.e., XAT, methyl radical capture, and S_H2 reductive elimination). Specifically, we envisioned that the first Ni precatalyst (**Ni-A**) would contain an electron-rich bipyridine ligand, like 4,4′-Me_2N-bpy (**L1**), and two bromine X-type ligands that would facilitate facile reduction by the photocatalyst to form an active $(bpy)Ni^{I}(Br)$ catalyst capable of activating the α-chloroamide via XAT.[31] The second Ni catalyst (**Ni−B**) would feature a scorpionate-type ligand, such as Tp*, and an acac X-type ligand, which together would facilitate the capture and stabilization of methyl radical prior to it either adding to the **Ni-A** center for inner-sphere coupling or undergoing S_H2 C−C bond formation at the **Ni−B** center with a cage-escaped alkyl halide radical. Indeed, we were pleased to find that the combination of 1.25 mol % $NiBr_2$·glyme/4,4′-Me_2N-bpy (**L1**) and 0.75 mol % $Ni(acac)_2$/KTp* (**L4**) led to a sizable improvement in yield (80% yield, Figure 6B, entry 1) compared to the previous plateaued conditions (entry 2). Notably, this dual Ni catalyst system maintained the same total Ni loading (2 mol %) compared to the single Ni system, thus supporting the role of catalytic cooperativity in yield enhancement. Minor adjustments to the **Ni-A**/**Ni−B** ratio (e.g., entry 3) resulted in a slightly lower yield. The choice of bpy ligand had a significant impact on reactivity, with more donating **L1** outperforming **L2** (entry 4) and **L3** (entry 5). The benefit of the unconventional ligand **L1**, which has not been employed in prior $C(sp^3)$−$C(sp^3)$ cross-couplings, over **L2** and **L3** may stem from its ability to produce a more electron-rich Ni center better-suited for activating alkyl chlorides.[39] Exclusion of **L4** from **Ni−B** (entry 6) also had a negative impact on cross-coupling, resulting in a yield of 69% compared to the optimal yield of 80% with **L4** present. Furthermore, a series of control studies (entry 7) revealed the

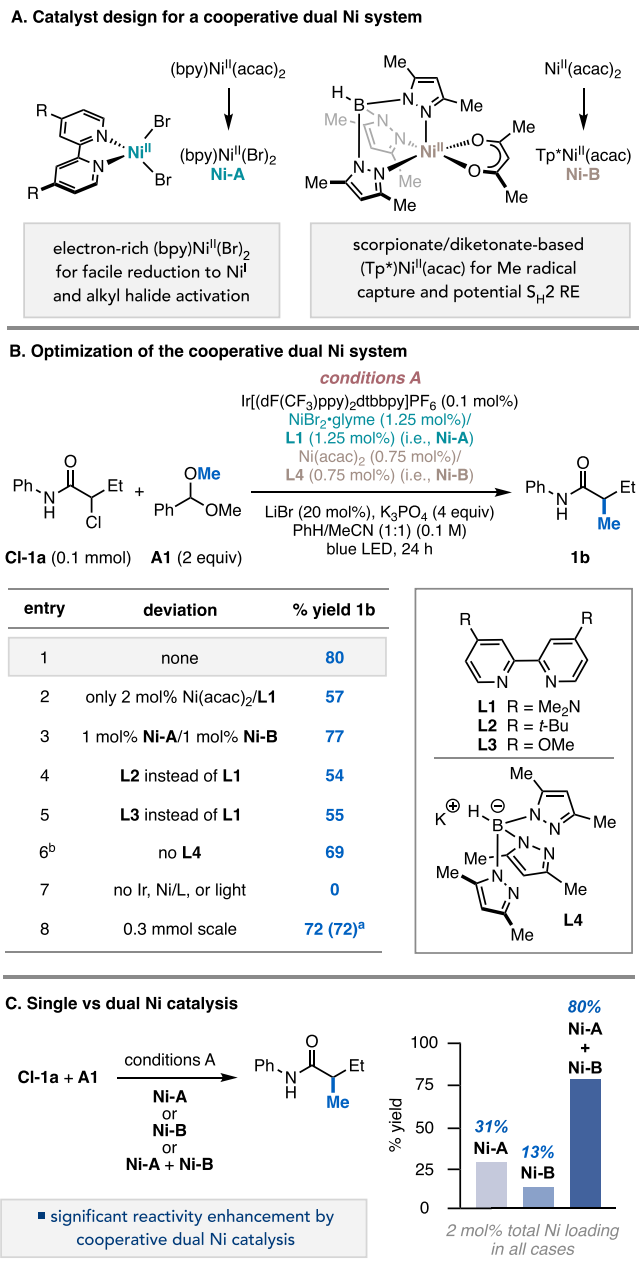

Figure 6. Development of a cooperative dual Ni catalysis strategy for $C(sp^3)$−chloride methylation. (A) Design of Ni cocatalysts. (B) Reaction optimization. (C) Evaluation of single Ni vs dual Ni catalysis. All yields determined by GC-FID analysis using 1,3,5-trimethoxybenzene as an external standard. [a]Isolated yield.

necessity for photocatalyst, Ni catalysts, and light in these cross-couplings. Finally, the need for both Ni catalysts was further examined by assessing the effect on yield when each Ni catalyst was excluded (Figure 6C). Exclusion of $Ni(acac)_2$/**L4** while maintaining the total catalyst loading from the standard conditions by using 2 mol % $NiBr_2$·glyme/**L1**, led to a large reduction in yield (31% yield) relative to the optimal 80% obtained using both Ni catalysts. Conversely, excluding $NiBr_2$·glyme/**L1** instead while using 2 mol % $Ni(acac)_2$/**L4** proved to be even less effective, resulting in a yield of just 13%.

Having demonstrated the effectiveness of the dual Ni catalytic strategy in the methylation of α-chloroamide **1a**, we began evaluating the scope of the $C(sp^3)$−methylation with respect to α-halo carbonyl derivatives (Figure 7). Using

https://doi.org/10.1021/jacs.5c10906
J. Am. Chem. Soc. XXXX, XXX, XXX−XXX

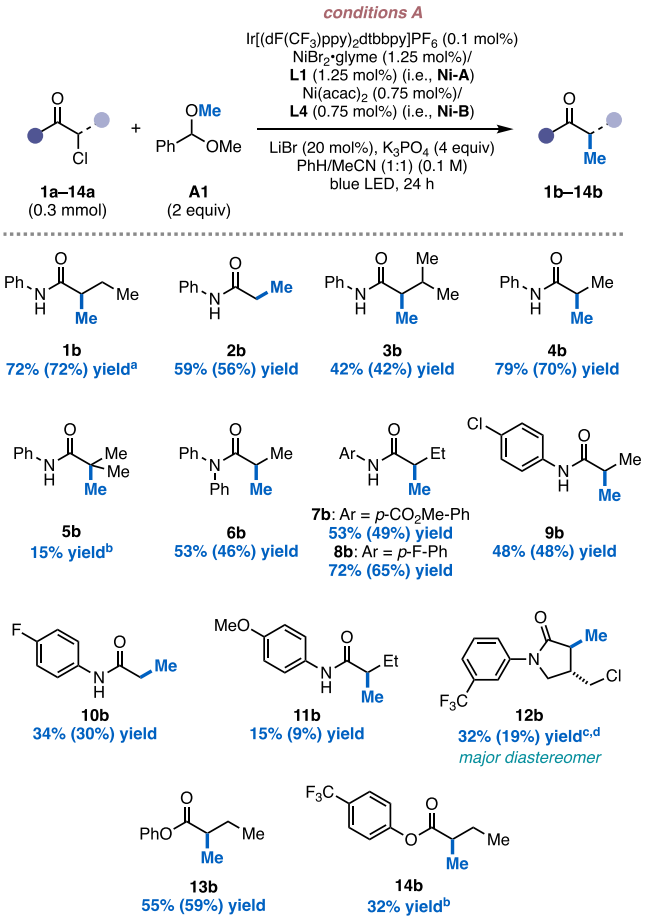

Figure 7. Scope of the dual Ni-catalyzed alkyl chloride methylation. The yields were determined by ^{1}H NMR or ^{a}GC-FID analysis using either 1,3,5-timethoxybenzene or mesitylene as an external standard and are an average of two trials. Isolated yields are shown in parentheses. ^{b}Isolated yields could not be obtained due to inseparable impurities (see Supporting Information Section 4.3 for details). ^{c}0.1 mmol scale. ^{d}Isolated as the major diastereomer. The minor diastereomer could not be isolated to determine an accurate d.r (see Supporting Information Section 4.3 for details).

conditions A, a variety of *N*-Ph-*α*-chloroamides bearing alkyl substituents with diverse steric profiles (**1a**−**4a**) were tolerated well in the reaction, delivering the corresponding methylated products (**1b**−**4b**) in moderate to high yield. We were pleased to find that tertiary chloro-amide **5a** underwent successful methylation as well, albeit in a lower yield. Bis-arylated amide **6a** was also successful in the transformation, indicating that *N*−Ni coordination is likely not necessary for reactivity and further highlighting the amenability of the cross-coupling to sterically demanding substrates. Furthermore, the methylation was tolerant to a variety of substituents on the *N*-aryl group, with electron deficient amides (**7a**−**10a**) performing significantly better than an electron-rich amide (**11a**), presumably due to enhanced activation of the C−Cl bond by inductively electron-withdrawing groups. Notably, the methylation of aryl-chloride-containing amide **9a** proceeded with complete selectivity for the alkyl chloride, leaving the aryl chloride motif intact. Complex amide **12a**, which contained both activated and unactivated alkyl chloride motifs, underwent site-selective methylation with modest diastereoselectively at the activated position to give product **12b**.

Gratifyingly, methylation of *α*-chloro esters **13a** and **14a** was also possible, showcasing the generality of the coupling across different classes of carbonyl derivatives. While methylation alpha to carbonyls is traditionally achieved via enolate alkylation, the strong base required for enolization poses selectivity challenges, leading to N− or O−alkylation or overalkylation at the *α*-carbon. Forming analogous products from *α*-chloroamides and esters, which remain highly underutilized substrates in Ni/photoredox radical methylation, circumvents such challenges.[40] Thus, this work showcases the power of strategic catalyst design in expanding the repertoire of electrophiles for radical-based coupling, which overall enables entry to unique structural motifs that complement those accessible by prior methods.

Having identified optimal conditions for the methylation of a diverse set of *α*-chloroamides using a dual Ni catalytic system, we returned to evaluate the general applicability of this method for the methylation of alkyl bromides. Given the observation during early optimization studies that more activated alkyl bromides are prone to photocatalytic reduction under the reaction conditions (vide supra), we sought to evaluate the effectiveness of unactivated alkyl bromides instead. Furthermore, we envisioned that by extending this methodology to two distinct alkyl halide classes we could accomplish the goal of obtaining even greater structural diversity in methylated products compared to previous methods.[10,12] Gratifyingly, we found that this dual Ni catalysis strategy could extend to unactivated bromides as well (i.e, **15a**, Figure 8A). While the standard chloride coupling conditions (i.e., conditions A and Figure 6B) provided the desired methylated product (**15b**) in 8% yield (Figure 8A, entry 1), minor adjustments to catalyst loadings and use of dtbbpy (**L2**) instead of **L1** produced **15b** in a much improved 78% yield (entry 2). In this case, more donating ligands like **L1** (entry 3) and **L3** (entry 4) proved to be less effective than **L2**. While bromide **15a** required higher photocatalyst and Ni catalyst loadings compared to chloride **1a**, the same relative ratio of **Ni−A** to **Ni−B** was found to be optimal for both reactions (entries 5 and 6), indicating a common mechanism across different alkyl halide classes. Control studies (entry 7) confirmed the necessity for photocatalyst, Ni catalysts, and light in the methylation of alkyl bromides, as in the case of *α*-chloroamides. For alkyl bromide **15a**, trials excluding one Ni catalyst (Figure 8B) were also met with a significant decrease in yield (50% and 41% vs the optimal 78%), similar to the alkyl chloride coupling. Overall, these results support the proposal of two discrete Ni catalysts cooperatively enhancing productive coupling.

Given the wide commercial availability of unactivated alkyl bromides and the diverse chemical space that they encompass, we applied our previously disclosed dimensionality reduction/clustering workflow to design and survey a diverse array of alkyl bromides (Figure 9, see Supporting Information Section 5.2 for details).[12,17,41] While the alkyl bromides selected from this workflow were somewhat structurally simple, they nonetheless were representative of all commercially available unactivated alkyl bromides and enabled comprehensive coverage of the chemical space. Guided by this approach, we explored the methylation of a broad range of medicinally relevant, unactivated alkyl bromides using conditions B. Both primary and secondary piperidine-containing alkyl bromides with *N*-Boc and *N*-Cbz protecting groups (**15a**−**17a**) underwent successful methylation in moderate to high yield.

https://doi.org/10.1021/jacs.5c10906
J. Am. Chem. Soc. XXXX, XXX, XXX−XXX

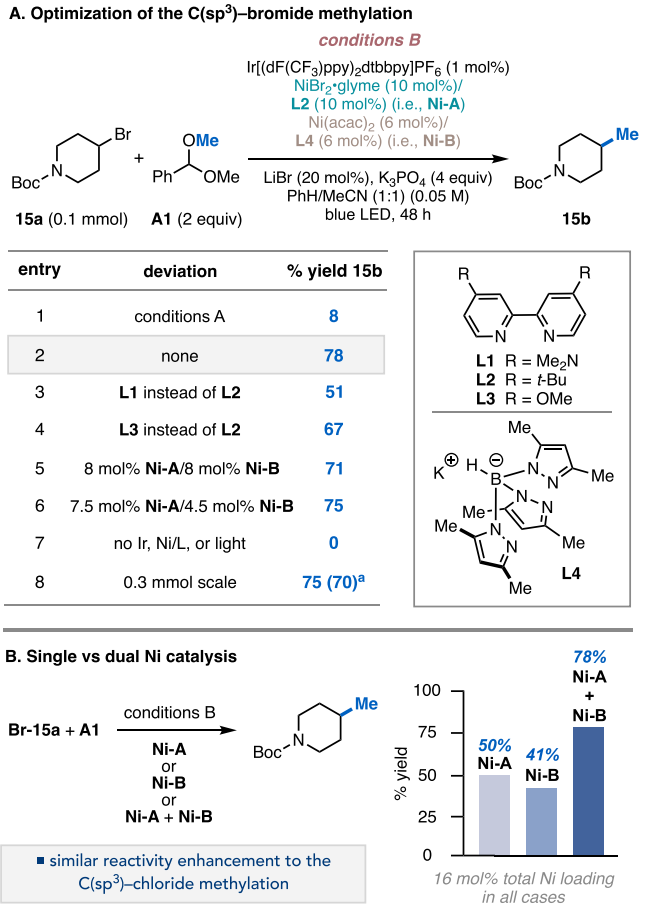

Figure 8. Development of the alkyl bromide methyl radical coupling using the cooperative dual Ni catalysis strategy. (A) Reaction optimization. (B) Evaluation of single Ni vs dual Ni catalysis. All yields determined by ^{1}H NMR or GC-FID analysis using 1,3,5-trimethoxybenzene as an external standard. [a]Isolated yield.

Additional saturated heterocycles, including morpholine **18a**, tetrahydropyran **19a**, cyclobutane **20a**, and azetidine **21a** were also well-tolerated under the reaction conditions to give a diverse array of methylated products (**18b**–**21b**) in good yield. Enantioenriched butyrolactam **22a** delivered methylated product **22b** without loss of enantiomeric excess, thus highlighting the stability of stereocenters—even those with adjacent heterofunctionality that may promote undesired HAT—under the reaction conditions. Primary alkyl bromides tethered to pyrazole (**23a**), phthalimide (**24a**), and aryl chloride (**25a**) functionality were also successful in the transformation, with **23a** and **25a** showing exclusive selectivity for methylation at the C(sp^3)–Br position over the C(sp^2)–Cl position. Furthermore, primary alkyl bromides containing alkyl chloride (**26a**) and ester (**27a**) moieties, as well as acyclic secondary alkyl bromide **28a**, also underwent efficient methylation under the reaction conditions. Importantly, while conditions B proved to be the most general across diverse alkyl halides with differing substitution patterns, lower Ni loadings (8% total) and reaction times (24 h) could be used for some primary alkyl halides, like **24a**, to achieve identical yields (Figure 10A, entries 1 and 2), while secondary alkyl halides, like **15a**, require the standard reaction conditions to reach optimal yields (Figure 10A, entries 3 and 4). Unfortunately, tertiary alkyl bromides like **29a**–**31a** (Figure 9) did not undergo productive methylation (See Supporting Information Section 5.2 for details). Given the importance of methyl groups as bioisosteres, we next turned our attention to applying the coupling to biologically relevant molecules. Gratifyingly, we found that nucleoside **32a** and monosaccharide **33a** could undergo cross-coupling to afford methylated products **32b** and **33b** in moderate yield. Importantly, these products represent complementary bioisosteres to fluorinated analogues that are accessible by a radical fluorination protocol established by MacMillan and co-workers.[42] Also notable is that given the activated nature of **33a**, the standard chloride conditions (i.e., conditions A, Figure 6) with 4,4′-F-bpy instead of **L1** proved to be more effective than conditions B for this specific cross-coupling. This result further underscores the flexibility of the method in accommodating substrates with differing electronic profiles through simple adjustments to the catalyst loadings and bipyridine ligand identity. Complex products derived from pharmaceuticals celecoxib (**34b**) and lenalidomide (**35b**) could also be accessed via methylation of the corresponding alkyl bromides, showcasing the amenability of this methodology to late stage functionalization. As one final test of the generality of the method, we applied conditions B to the methylation of 4-bromo acetophenone (**Ar-1a**, Figure 10B).[12] The methylated product (**Ar-1b**) was delivered in 74% yield without any modifications to the reaction conditions, highlighting a unified dual Ni catalysis approach to both alkyl halide and aryl bromide methylation. Overall, this radical methylation strategy enables selective methylation of a variety of substrates, including those containing nucleophilic functionality, such as amides (e.g., **22a**) and amines (e.g., **28a**), which may otherwise pose selectivity challenges in reactions that rely on MeI or MeOTs as a methylating agent.[43,44]

To further expand upon the diversity of alkyl–alkyl bonds formed under this catalytic regime, we next aimed to demonstrate the utility of the method in constructing C–C bonds with varying degrees of carbon substitution by strategically coupling primary bromide **24a** and secondary bromide **15a** with various acetal-derived primary and secondary alkyl radicals (Figure 11). Beginning with acetal **A2**, deuteromethylation of primary bromide **24a** occurred to produce **36** in a high yield. Following minor changes to the reaction conditions (see Supporting Information Section 3.3), other primary radicals derived from acetals **A3**–**A5** underwent successful coupling with primary bromide **24a** to forge new primary–primary alkyl bonds (**37**–**39**) with minimal homocoupling (8%) of **24a**. Next, coupling between secondary alkyl bromide **15a** and primary acetals **A2**–**A5** enabled access to a set of alkylated products (**40**–**43**) with secondary–primary alkyl bonds. Secondary acetals **A6** and **A7**, which can be readily derived from isopropanol and cyclopentanol, were also evaluated. The coupling between primary alkyl bromide **24a** and these secondary acetals provided **44** and **45** in moderate yield. Lastly, more challenging secondary–secondary cross-couplings proved to be feasible as well, with coupling between bromide **15a** and acetals **A6** and **A7** providing **46** and **47**, albeit in lower yields. Overall, this approach provides a unified method for the methylation and alkylation of diverse primary and secondary chlorides and bromides, which enables rapid diversification and exploration of high fraction sp^3 small molecules originating from diverse alkyl halide classes.

Mechanistic Analysis. Given the unusual dependence of this chemistry on two distinct Ni catalysts and the mechanistic complexities underlying Ni/photoredox-catalyzed C(sp^3)–C(sp^3) cross-coupling, we sought to gain a deeper under-

https://doi.org/10.1021/jacs.5c10906
J. Am. Chem. Soc. XXXX, XXX, XXX–XXX

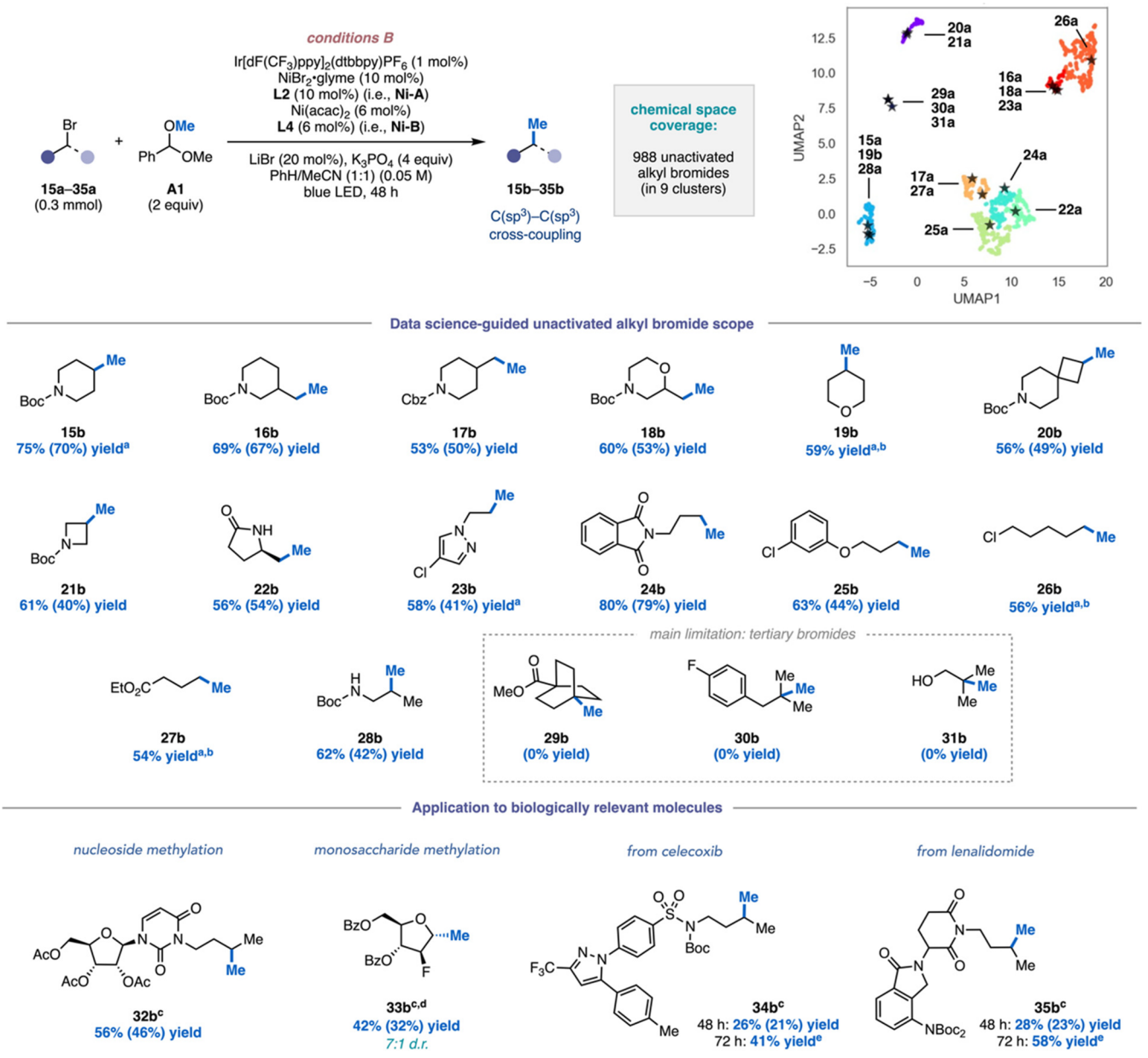

Figure 9. Scope of the methyl radical coupling with unactivated alkyl bromides selected through a data science-guided approach and application of the cross-coupling to biologically relevant molecules. For methylation of alkyl bromide substrates, the total catalyst loading (16 mol %) was added in two equal portions (8 mol % and 8 mol %), with the second portion being added after the first 24 h. The yields were determined by ^{1}H NMR or [a]GC-FID analysis using either 1,3,5-timethoxybenzene or mesitylene as an external standard and are an average of two trials. Isolated yields are shown in parentheses. [b]Due to volatility, these substrates could not be isolated (see Supporting Information Section 5.3 for details). [c]0.1 mmol scale. [d]Conditions A with 4,4′-F-bpy used instead. [e]After 48 h, an additional 8 mol % of Ni catalyst was added and the reactions were run for 72 h.

standing of our leading mechanistic hypothesis: cooperativity between XAT, S_H2, and inner-sphere coupling cycles (mechanism 2, Figure 5B). Specifically, we aimed to interrogate: (1) the reduction of (bpy)Ni^{II}(X)$_2$ to (bpy)Ni^{I}(X) compared to the reduction of (Tp*)Ni^{II}(acac) to (Tp*)Ni^{I}, (2) the sequence of elementary steps of the inner-sphere coupling process, and (3) the effect of the acetal-derived alkyl radical on the pathway for C−C bond formation (inner-vs outer-sphere coupling). Based on the design of the dual Ni catalytic system, a single electron transfer (SET) reduction of Ni^{II} to Ni^{I} by the reduced Ir^{II} photocatalyst must occur for productive reactivity. Given that **Ni−A** features a redox active bpy ligand and two bromide X-type ligands, we hypothesized that this species would be more easily reduced to Ni^{I} than **Ni−B**, in accordance with mechanism 2 (Figure 5B). Indeed, pulse radiolysis[45] experiments at Brookhaven National Laboratory's Laser Electron Accelerator Facility[46] (see Supporting Information Section 7.4 for details) revealed the kinetic favorability of **Ni−A** reduction over **Ni−B** via SET from Ir^{II} (Figure 12). The rate constant of $4.2 \pm 0.3 \times 10^{7}$ M^{-1} s^{-1} for SET from Ir^{II} to **Ni−A** was found to be in good agreement with that recently reported by Sayre[47] under similar conditions, and shown here to be at least 40 times faster than SET to **Ni−B**. This provides evidence for a proposal in which (bpy)-Ni^{I}(Br) is generated and free to facilitate alkyl halide activation (via XAT) for outer-sphere coupling as well as participate in an

https://doi.org/10.1021/jacs.5c10906
J. Am. Chem. Soc. XXXX, XXX, XXX−XXX

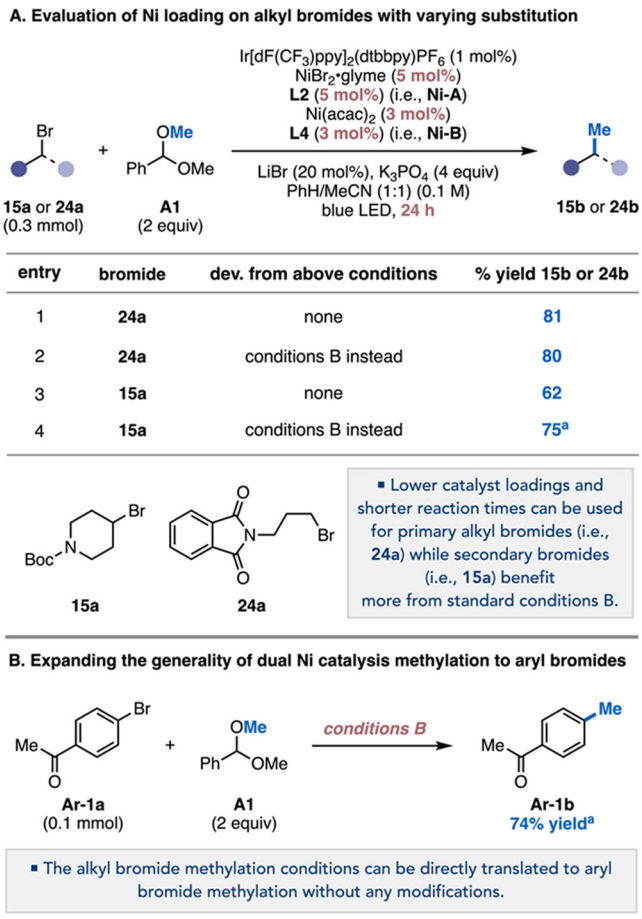

Figure 10. (A) Evaluating the effect of Ni loading on alkyl bromides with varying substitution, (B) direct application of alkyl bromide methylation conditions to aryl bromide methylation. For conditions B, the total catalyst loading (16 mol %) was added in two equal portions (8 mol % and 8 mol %), with the second portion being added after the first 24 h. The yields were determined by ^{1}H NMR or ^{a}GC-FID analysis using either 1,3,5-timethoxybenzene or mesitylene as an external standard.

inner-sphere C−C bond forming cycle (i.e., mechanism 2, Figure 5B).

Next, we sought to decipher the sequence of elementary steps in the inner sphere cross-coupling cycle facilitated by (bpy)Ni^{I}(Br). In prior Ni/photoredox-catalyzed C(sp^2)−C(sp^3) cross-couplings of aryl halides and alkyl radicals, a common mechanistic proposal involves rapid activation of the aryl halide (via a concerted oxidative addition mechanism) by a (bpy)Ni^{I}(X) catalyst followed by SET reduction to form a relatively stable (bpy)Ni^{II}(Ar)(X) intermediate prior to alkyl radical capture.[38,48−51] However, due to the comparatively less reactive C(sp^3)−X bond in alkyl halides, we postulated that the rate of alkyl halide activation by (bpy)Ni^{I}(X) (via an XAT mechanism) may be slow enough to compete with the rate of acetal-derived radical addition to (bpy)Ni^{I}(X). As such, we sought to gain insight into whether XAT or radical addition occurs first at the (bpy)Ni^{I}(Br) catalyst (Figure 13A). We hypothesized that if addition of an acetal-derived isopropyl radical to Ni were to occur before alkyl halide activation, isomerization of the isopropyl fragment via β-H elimination/migratory insertion would occur at the (bpy)Ni^{II}(*i*-Pr)(Br) center (Figure 13B).[10] Subsequent reduction of the resulting (bpy)Ni^{II}(*i*-Pr)(X) and (bpy)Ni^{II}(*n*-Pr)(X) species by Ir^{II}

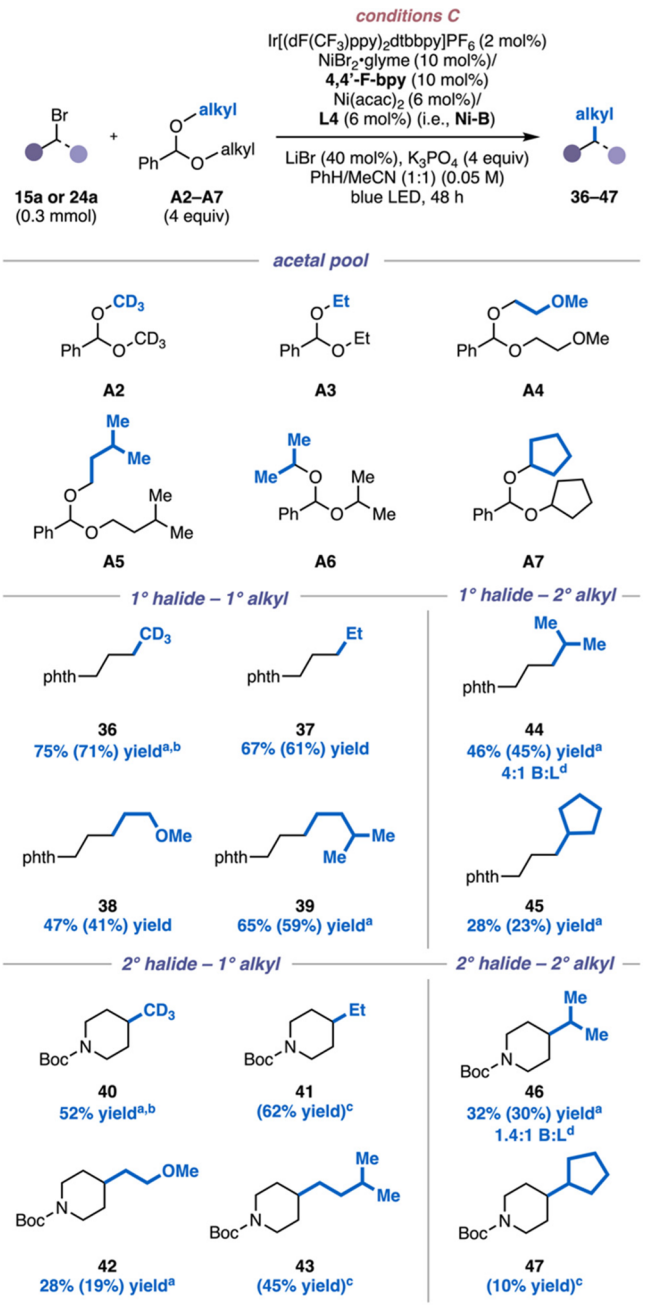

Figure 11. Diverse alkyl−alkyl bond formations. The yields were determined by ^{1}H NMR or ^{a}GC-FID analysis using either 1,3,5-trimethoxybenzene or mesitylene as an external standard and are an average of two trials. Isolated yields are shown in parentheses. ^{b}Conditions B (0.1 mmol scale, dtbbpy instead of dFbpy, 2 equiv. **A2**, 20 mol % LiBr) were used instead. ^{c}Average of two isolated yields. ^{d}Branched (**B**) to linear (**L**) ratios were determined by GC-FID analysis using either 1,3,5-trimethoxybenzene or mesitylene as an external standard; only major isomer (**B**) shown. For all trials, the total catalyst loading (16 mol %) was added in two equal portions (8 mol % and 8 mol %), with the second portion being added after the first 24 h.

would yield (bpy)Ni^{I}(*i*-Pr) and (bpy)Ni^{I}(*n*-Pr) intermediates, which would then engage in XAT activation of the alkyl halide, followed by radical rebound and reductive elimination to afford branched and linear isomeric products. To assess this proposal, we evaluated the coupling of alkyl bromide substrates **24a** and **15a** with the isopropyl acetal **A6** (Figure 13C). In both cases,

https://doi.org/10.1021/jacs.5c10906
J. Am. Chem. Soc. XXXX, XXX, XXX−XXX

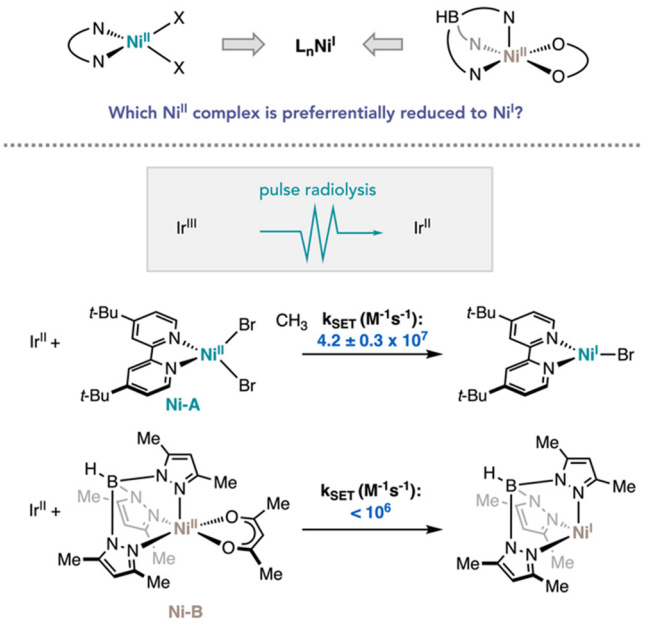

Figure 12. Kinetics of Ni^{II} reduction by Ir^{II}, initiated by reduction of Ir^{III} by solvated electrons from pulse radiolysis experiments in acetonitrile (see Supporting Information Section 7.4 for details).

we observed the formation of branched and linear coupled products, thus supporting this isomerization proposal.

Additionally, density functional theory (DFT)-based calculations (Figure 13D) at the (U)B3LYP-D3/def2-TZVP/CPCM(MeCN)//(U)B3LYP-D3/def2-SVP/CPCM(MeCN) level of theory (see Supporting Information Figure S32 for details) revealed the kinetic barrier for methyl radical addition to (bpy)Ni^{I}(Br) ($\Delta G^{\ddagger}$ = 7.7 kcal/mol) to be lower than that of XAT by (bpy)Ni^{I}(Br) ($\Delta G^{\ddagger}$ = 18.6 kcal/mol), further corroborating the proposed sequence of elementary steps shown in Figure 13B in which radical addition occurs before XAT.

With evidence in hand supporting a "radical addition first" mechanism at the (bpy)Ni^{I}(Br) inner-sphere cycle, we next turned our attention to further interrogating this full sequence of elementary steps computationally (Figure 14). Beginning at the putative (bpy)Ni^{I}(Br) species (^{2}**Int-2**), we first considered a scenario in which X-type ligand exchange could give rise to a second Ni^{I} species ((bpy)Ni^{I}(acac), ^{2}**Int-2′**) that could also facilitate cross-coupling (Figure 14A). Calculations ultimately revealed a thermodynamic preference of 2.8 kcal/mol for (bpy)Ni^{I}(Br) over (bpy)Ni^{I}(acac). Furthermore, the apparent barrier for the addition of a methyl radical to (bpy)Ni^{I}(Br) ($\Delta G^{\ddagger}$ = 7.7 kcal/mol) is 1.7 kcal/mol lower than that of addition to (bpy)Ni^{I}(acac) ($\Delta G^{\ddagger}$ = 9.4 kcal/mol). Thus, we posit the selective formation of (bpy)Ni^{II}(Me)(Br) (^{1}**Int-3** or ^{3}**Int-3**). While radical addition initially affords square planar singlet (bpy)Ni^{II}(Me)(Br) (^{1}**Int-3**), facile intersystem crossing to the thermodynamically favored triplet spin state yields tetrahedral ^{3}**Int-3** (ΔG = − 1.4 kcal/mol).[52] While ^{3}**Int-3** is computed to be enthalpically favored by 1.2 kcal/mol over ^{1}**Int-3**, the spin distribution of **Int-3** is postulated to be temperature dependent (see Supporting Information Figure S32). At this stage, ^{3}**Int-3** (or ^{1}**Int-3**) is well poised to undergo SET from the reduced photocatalyst (^{2}**Ir^{II}**), affording (bpy)-

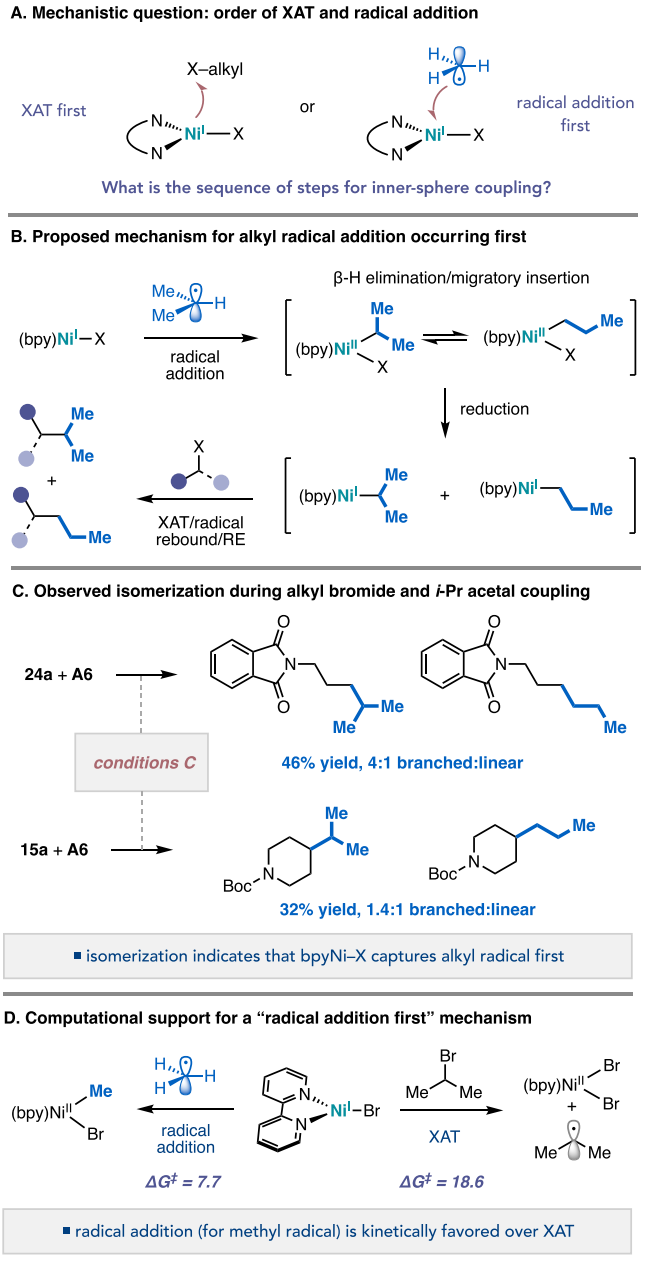

Figure 13. Evidence for a "radical addition first" mechanism. Yields and branched to linear ratios were determined by GC-FID analysis using either 1,3,5-trimethoxybenzene or mesitylene as an external standard. Reactions performed on 0.3 mmol scale. Calculations performed at the (U)B3LYP-D3/def2-TZVP/CPCM(MeCN)//(U)-B3LYP-D3/def2-SVP/CPCM(MeCN) level of theory.

Ni^{I}(Me) (^{2}**Int-4**) and regenerating LiBr ($\Delta G^{\ddagger}$ = 7.0 kcal/mol from ^{3}**Int-3**, $\Delta G^{\ddagger}$ = 3.8 kcal/mol from ^{1}**Int-3**, see Supporting Information Figure S33). Given the possibility of rapid Br/acac ligand exchange at ^{3}**Int-3**, the analogous process from (bpy)Ni^{II}(Me)(acac) (^{3}**Int-3′**) was also considered. In this case, however, the formation of (bpy)Ni^{II}(Me)(acac) is disfavored by 1.7 kcal/mol and bears a higher energetic penalty to reduction. Hence, we posit the reduction of (bpy)Ni^{II}(Me)(Br) (^{3}**Int-3**) to be the catalytically relevant process in the inner-sphere cycle.

Having established the energetic preference for the putative (bpy)Ni^{I}(Br) catalyst undergoing radical capture and reduction, we next sought to computationally investigate the

https://doi.org/10.1021/jacs.5c10906
J. Am. Chem. Soc. XXXX, XXX, XXX−XXX

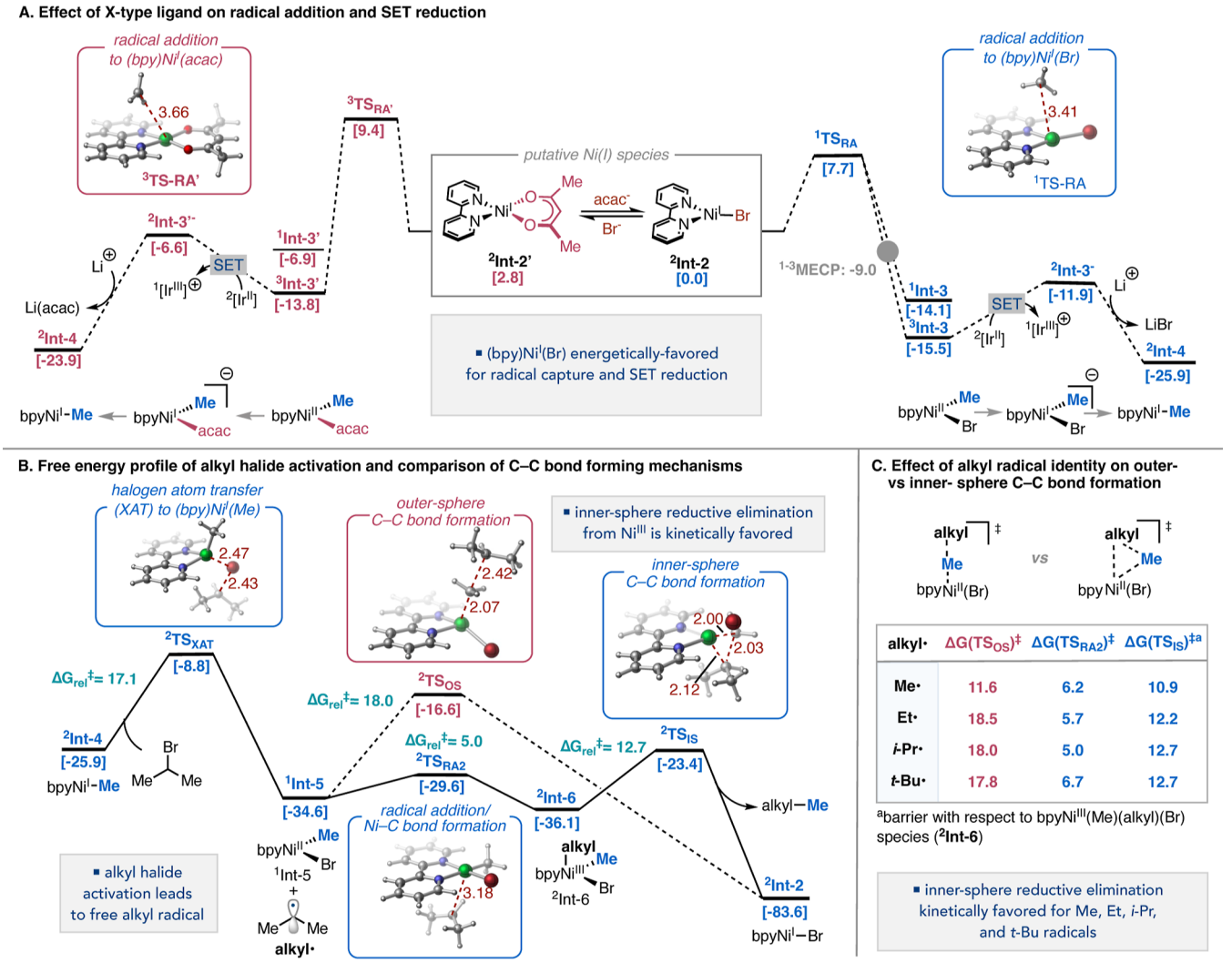

Figure 14. Computational analysis of the C(sp^3)–C(sp^3) cross-coupling. (A) Effect of X-type ligand on the energetics (free energies in kcal/mol) of radical addition and SET reduction (calculations performed at the (U)B3LYP-D3/def2-TZVP/CPCM(MeCN)//(U)B3LYP-D3/def2-SVP/CPCM(MeCN) level of theory. (B) Free energy profile for alkyl halide activation and comparison of C–C bond forming mechanisms. (C) Effect of alkyl radical identity on outer-versus inner-sphere C–C bond formation. MECP, minimum energy crossing point.

energetics of the XAT process and confirm that C(sp^3)–C(sp^3) bond formation at the (bpy)Ni catalyst occurs via an inner-sphere mechanism (Figure 14B). For this analysis, we used a secondary alkyl bromide (i.e., *i*-Pr–Br) as the cross-coupling partner. Calculations revealed that (bpy)Ni^I(Me) (^{2}**Int-4**) can promote alkyl halide activation (via $\mathbf{TS_{XAT}}$) with a modest barrier of 17.1 kcal/mol, resulting in a (bpy)Ni^{II}(Me)-(Br) singlet species (^{1}**Int-5**) and an isopropyl radical (**alkyl•**) ($\Delta G = -8.7$ kcal/mol). At this stage, quasiclassical molecular dynamics simulations initialized from $\mathbf{TS_{XAT}}$ suggested free diffusion of this alkyl radical rather than immediate rebound to ^{1}**Int-5** following XAT (see Supporting Information Figure S39).[29,31] Given this finding, we decided to evaluate the energy profiles of both the outer- and inner-sphere C(sp^3)–C(sp^3) bond-forming processes. While these studies unveiled that the outer-sphere C–C bond forming mechanism (via $\mathbf{TS_{OS}}$) is energetically tractable under the reaction conditions (barrier of 18.0 kcal/mol), they ultimately revealed inner-sphere C–C bond formation to be lower in energy. Specifically, this pathway involves facile radical addition to ^{1}**Int-5** ($\Delta G^{\ddagger} = 5.0$ kcal/mol) to afford a Ni^{III} intermediate (^{2}**Int-6**) that then undergoes inner-sphere reductive elimination via $\mathbf{TS_{IS}}$ (barrier of 12.7 kcal/mol) to forge the desired C(sp^3)–C(sp^3) cross-coupled product and regenerate (bpy)Ni^I(Br) (^{2}**Int-2**) for the $Ni^I/Ni^{II}/Ni^I/Ni^{II}/Ni^{III}$ catalytic cycle. Notably, the energetic preference for inner-sphere coupling at the $(L)_nNi^I$(Br) complex is consistent with the enantioinduction observed when using a chiral ligand during optimization studies (Figure 5C); however, it is important to note that these computational studies may not fully capture the mechanism in that case since those studies relied on a tridentate ligand. Next, to evaluate if the outer-sphere mechanism would be operative with different alkyl bromides, we computed the competing barriers (i.e., $\mathbf{TS_{OS}}$, $\mathbf{TS_{RA2}}$, and $\mathbf{TS_{IS}}$) for outer-versus inner-sphere C–C bond formation for a range of representative alkyl radicals (Figure 14C). Notably, the outer-sphere pathway was found to be higher in energy in all cases. Additionally, the barrier for inner sphere Me–Me reductive elimination (10.9 kcal/mol), which is lower relative to other alkyl–Me reductive eliminations, may be consistent with a proposal in which competitive off-cycle methyl homocoupling occurs in the absence of the (Tp*)Ni^{II}(acac) cocatalyst. Finally, modeling of *α*-chloro-*N*-phenylacetamide in the cross-coupling revealed an

https://doi.org/10.1021/jacs.5c10906
J. Am. Chem. Soc. XXXX, XXX, XXX–XXX

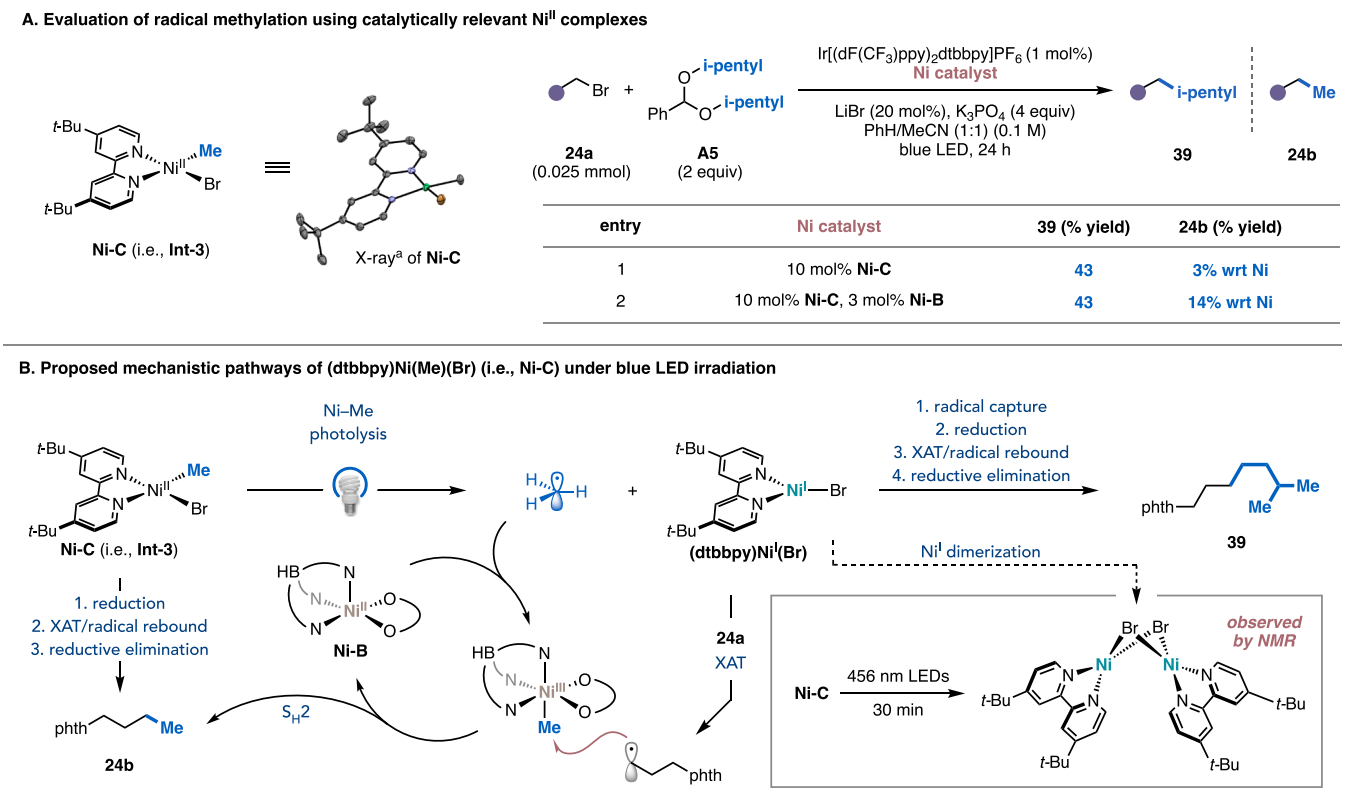

Figure 15. (A) Synthesis and catalytic competency of (dtbbpy)Ni^{II}(Me)(Br) (i.e., **Ni−C**). All yields were determined by GC-FID analysis using either 1,3,5-trimethoxybenzene or mesitylene as an external standard. [a]ORTEP rendering showing ellipsoids at 50% probability with hydrogen atoms omitted for clarity. (B) Productive off-cycle pathways for (dtbbpy)Ni(Me)(Br) (i.e., **Ni−C**). Wrt, with respect to **Ni−C**.

identical and feasible Ni^{I}/Ni^{II}/Ni^{I}/Ni^{II}/Ni^{III} catalytic cycle for the inner-sphere process (see Supporting Information Figure S40). Overall, these computational studies further support the feasibility of C(sp^3)−C(sp^3) coupling via an inner-sphere mechanism involving radical addition, reduction, XAT, radical rebound, and Ni^{III} reductive elimination.

While this sequence of elementary steps has been proposed in prior Ni-catalyzed C(sp^3)−C(sp^3) cross-couplings,[40,53] such mechanisms have been traditionally difficult to probe experimentally given the reactive and unstable nature of many catalytically relevant Ni^{I}, Ni^{II}, and Ni^{III} complexes. Despite the synthetic challenges that such species pose, we set out to prepare one of the intermediates in the proposed inner-sphere coupling mechanism to probe its reactivity in the cross-coupling reaction. Specifically, we envisioned preparing a (dtbbpy)Ni^{II}(alkyl)(Br) complex and subjecting it to catalytic experiments. Given the focus of this method on alkyl halide methylation and its lack of β-hydrogens, we chose to prepare (dtbbpy)Ni^{II}(Me)(Br) (**Ni−C**, **Int-3**, Figure 15A). By treating (dtbbpy)Ni^{II}(Me)$_2$[54] with Et$_3$N·HBr, methane could be liberated in a protodemetalation reaction. Recrystallization of the crude material from THF/pentane afforded bright red crystals of **Ni−C•pentane**. This complex was structurally characterized by single-crystal X-ray diffraction, revealing a pseudosquare planar Ni center (see Supporting Information Section 7.6 for experimental details). Furthermore, the ^{1}H NMR spectrum of **Ni−C** in CD$_3$CN features coalescence of the *t*-Bu signals, suggesting a rapid interconversion between square planar and tetrahedral geometries. These experimental results are in accord with a small adiabatic singlet−triplet gap, in alignment with computations that suggest that reduction may occur from either ^{1}**Int-3** or ^{3}**Int-3**. Despite being commonly invoked intermediates in prior alkyl−alkyl cross-couplings,[40,53] this marked the first synthesis, isolation, and characterization of a (bpy)Ni^{II}(alkyl)(X) complex with a nonbenzylic alkyl group.[55]

With **Ni−C** in hand, we next aimed to provide further experimental support for the inner-sphere mechanism involving (1) the reduction of (bpy)Ni^{II}(alkyl)(X) to (bpy)-Ni^{I}(alkyl)(X), (2) XAT/radical rebound, and (3) reductive elimination (Figure 14). Toward this goal, we performed a crossover-type experiment, using 10 mol % **Ni−C** as a catalyst in the cross-coupling of alkyl bromide **24a** and *i*-pentyl acetal **A5** in the absence (entry 1) and presence (entry 2) of **Ni−B**. In both cases, the *i*-pentyl coupled product (**39**) was obtained in 43% yield, corresponding to four turnovers of **Ni−C**. Interestingly, both cases delivered relatively low yields of methylated product **24b** (3% yield with respect to **Ni−C** in the absence of **Ni−B** (entry 1) and 14% yield with respect to **Ni−C** in the presence of 3 mol % **Ni−B** (entry 2)). While formation of the methylated product nonetheless provided support for the proposed sequence of elementary steps, low yields of **24b** and relatively high yields of **39** suggested that under these specific conditions, **Ni−C** may be susceptible to off-cycle pathways that still enable productive cross-coupling (Figure 15B). We hypothesized that light-induced photolysis of (dtbbpy)Ni^{II}(Me)(Br) could be generating methyl radical and (dtbbpy)Ni^{I}(Br), analogous to the formation of *o*-tolyl (*o*-Tol) radical via photolysis of (dtbbpy)Ni^{II}(*o*-Tol)(Cl).[56−58] In the absence of **Ni−B** (i.e., (Tp*)Ni^{II}(acac)), this methyl radical could escape the (dtbbpy)Ni^{I}(Br) solvent cage and form either methane or ethane. However, in the presence of **Ni−B** (i.e., entry 2, Figure 15A), this cage-escaped methyl radical could instead be captured by (Tp*)Ni^{II}(acac), which

https://doi.org/10.1021/jacs.5c10906
J. Am. Chem. Soc. XXXX, XXX, XXX−XXX

would facilitate outer-sphere C−C bond formation and lead to an increased yield of methylated product (See Supporting Information Section 7.6 for detailed discussion). This proposal is supported by ^{1}H NMR experiments which show that while **Ni−C** is stable in solution at room temperature under ambient light, irradiation of a solution of this complex in CD_3CN with 456 nm light results in the formation of $[(dtbbpy)Ni^I(Br)]_2$ by ^{1}H NMR, which presumably arises following homolysis of the Ni−Me bond and dimerization of the resultant (dtbbpy)-Ni^I(Br) complex (see Supporting Information Figure S31 for details). Overall, these results not only provide support for the intermediacy of (dtbbpy)Ni^{II}(Me)(Br) and (bpy)Ni^I(Br) but also show the potential off-cycle pathways that can still result in productive cross-coupling.

With a better understanding of the mechanistic features of the inner-sphere cross-coupling cycle, we aimed to understand the interplay between this inner-sphere pathway facilitated by reduced **Ni−A** and an outer-sphere pathway facilitated by both **Ni−A** and **Ni−B**. During optimization studies of the methylation reaction, we determined that the dual Ni catalyst system leads to higher yields for both alkyl chloride and alkyl bromide substrates (vide supra). Specifically, we found that for **Cl-1a**, the yield of the methylation was improved by including **Ni−B** (31% yield using just **Ni−A** vs 80% yield using **Ni−A** and **Ni−B**). Furthermore, the yield of methylation of **Br-15a** was also greater with inclusion of **Ni−B** (50% yield using just **Ni−A** vs 78% yield using **Ni−A** and **Ni−B**), albeit to a slightly lesser degree (Figure 16A). These results suggested to us that while cooperativity between outer- and inner-sphere coupling is important for both activated alkyl chloride substrates and unactivated alkyl bromides, the alkyl chlorides appear to depend more on the outer-sphere process for productive coupling. The preference for alkyl chlorides to engage in outer-sphere coupling (via XAT and S_H2) compared to alkyl bromides may be attributed to two factors: (1) the activated nature of the alkyl chlorides, which would be more susceptible to (bpy)Ni^I(Br)-catalyzed XAT, and (2) the greater stability of the resultant alkyl radical formed from the α-chloro carbonyl derivatives. This stabilized radical would be more likely to escape the solvent cage of the (bpy)Ni catalyst and engage in outer-sphere coupling with (Tp*)Ni^{III}(acac)(Me). These results also align with the greater propensity of the alkyl chlorides to undergo protodehalogenation (see Supporting Information Section 3)—presumably via XAT, cage-escape, and HAT—as well as the improved yields observed when using the electron-rich 4,4′-Me_2N-bpy ligand, which would enhance the rate of XAT. Interestingly, when electron-rich bpy ligands were used (i.e., 4,4′-Me_2N-bpy and 4,4′-OMe-bpy) as part of the dual Ni system for the alkyl bromides, yields significantly decreased (51−67% yield vs the optimal 78% yield when using dtbbpy instead). These results suggest that alkyl bromides may undergo inner- and outer-sphere radical methylation to a more equal extent compared to the α-chloro carbonyl derivatives, thus rendering cross-coupling of these substrates particularly sensitive to bpy ligands that are too electron-rich and, as a result, may promote (bpy)Ni^I(Br)-catalyzed XAT over radical addition to (bpy)Ni^I(Br).

Similar to Ni exclusion studies with different alkyl halides (Figure 16A), we also evaluated if changing the identity of the acetal-derived alkyl radical has any effect on what Ni species are required for productive coupling to gain further insight into the factors that make inner- or outer-sphere coupling preferable (Figure 16B). Computational studies revealed that

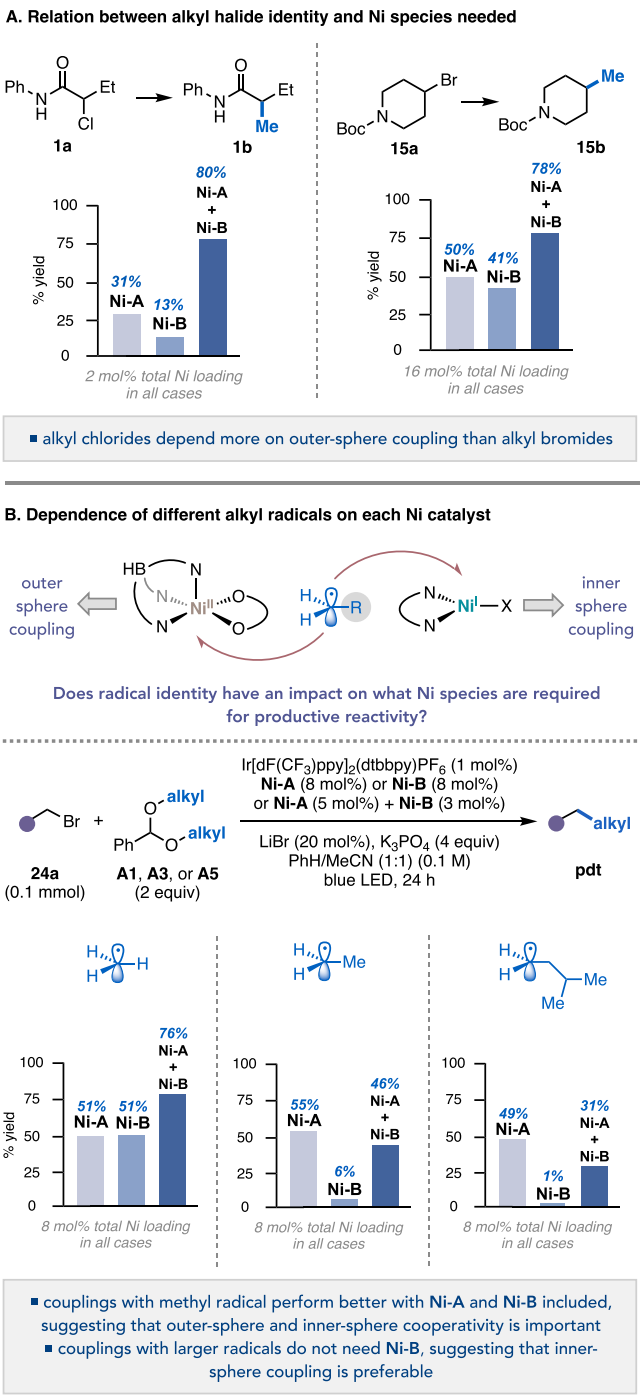

Figure 16. Impact of substrate structural features on the dependence of Ni species. (A) Exclusion of each Ni catalyst with each alkyl halide class. (B) Exclusion of each Ni catalyst with different acetal-derived alkyl radicals. All yields were determined by GC-FID analysis using either 1,3,5-trimethoxybenzene or mesitylene as an external standard.

as the steric profile of the alkyl group increases, the association of free alkyl radical to (Tp*)Ni^{II}(acac) becomes less thermodynamically favorable (see Supporting Information Figure S43 for details). These calculations are in line with previous studies that highlight a preference for methyl-radical capture at an analogous (Tp*)Ni(OAc) complex.[33] Accordingly, we hypothesized that couplings employing methyl radical should benefit more from the dual Ni catalyst system compared to nonmethyl radicals like ethyl and isopentyl

https://doi.org/10.1021/jacs.5c10906
J. Am. Chem. Soc. XXXX, XXX, XXX−XXX

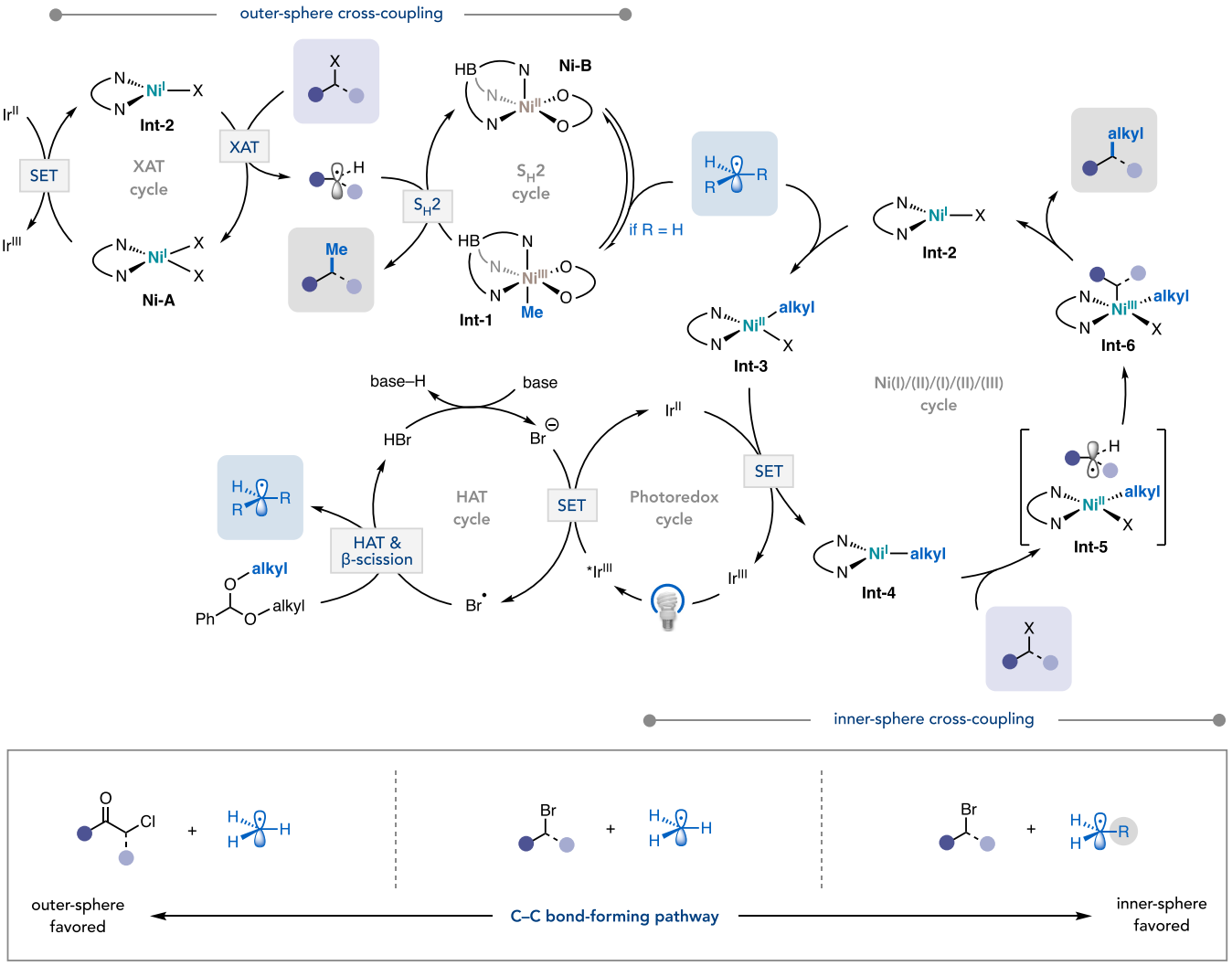

Figure 17. Proposed reaction mechanism and summary of preferred C−C bond-forming pathways for various substrate combinations.

radicals, due to the instability of methyl radical and its greater propensity to engage in radical capture and S_H2 at a Ni-diketonate complex.[32,34] To test this hypothesis, we performed similar Ni exclusion experiments for the cross-coupling of alkyl bromide **24a** with acetals **A1**, **A3**, and **A5**. It is important to note that while 4,4′-F-bpy was found to be the optimal ligand for coupling acetals other than **A1**, we chose to use dtbbpy—the optimal ligand for couplings with **A1**—in these studies so that direct comparisons could be made between methylation and other alkylations. For the coupling between **24a** and methyl radical, using just **Ni−A** or **Ni−B** delivered the product in 51% yield. In an analogous fashion to alkyl bromide **15a**, higher yields (76%) were achieved when using the dual Ni catalyst system. Contrary to the methyl radical coupling, using just **Ni−A** in the ethyl radical coupling gave higher yields (55%) compared to using just **Ni−B** (6%) or using **Ni−A** and **Ni−B** together (46%). For the isopentyl radical coupling, using just **Ni−A** also led to higher yields (49%) compared to using just **Ni−B** (1%) or **Ni−A** and **Ni−B** together (31%). These results indicate that for acetal-derived radicals (excluding methyl radical), the inner-sphere pathway, mediated by reduced **Ni−A**, is likely operative to a greater extent. This hypothesis aligns with the inclusion of **Ni−B** in these cases not producing the same positive effect that is exhibited in the methyl radical coupling, which occurs due to the methyl radical coupling having a greater dependence on cooperativity between outer- and inner-sphere cycles. In fact, inclusion of **Ni−B** provides a slightly negative impact on these reactions, which may be attributed to the ability of **Ni−B** to capture primary radicals such as ethyl and isopentyl radical, but not as effectively engage in outer-sphere C−C bond formation via S_H2. Moreover, when a more electron deficient bpy ligand (dFbpy) was employed in analogous exclusion studies, the inclusion of **Ni−B** did not appear to compete with alkyl radical capture to **Ni−A** and was not found to be detrimental to the yield of the reaction (see Supporting Information Table S36 for details). Lastly, it is important to note that we cannot completely rule out the possibility that (Tp*)Ni^{II}(acac) (**Ni−B**) may be serving a more supportive role in the methyl radical coupling by capturing and releasing reactive radical species (e.g., methyl radical), thereby stabilizing the radical and modulating its addition to the reduced **Ni−A** catalyst, akin to previous studies that have proposed leveraging a cocatalyst to prolong radical lifetime and enhance productive reactivity.[59] By controlling the rate of radical addition to the reduced **Ni−A** catalyst, this "radical reservoir" effect would preclude sequential radical additions to the reduced (bpy)Ni catalyst,

https://doi.org/10.1021/jacs.5c10906
J. Am. Chem. Soc. XXXX, XXX, XXX−XXX

thus enhancing productive coupling by mitigating off-cycle reactivity (e.g., homocoupling of the acetal-derived radical).

On the basis of these observations, we propose a mechanism centered around cooperativity between XAT, S_H2, and inner-sphere Ni cycles that begins with the Ir^{III}* triplet excited state oxidizing bromide to bromine radical ($E_{1/2}[Ir^{III}*/Ir^{II}]$ = +1.21 V vs SCE in MeCN; $E_{1/2}[Br^-/Br^\bullet]$ = +0.80 V vs SCE in dimethoxyethane),[60] which then facilitates HAT selectively at the tertiary C−H bond of the acetal (Figure 17).[10,12] In the case of methylation, subsequent β-scission would liberate methyl radical that is free to either associate reversibly with **Ni−B** for outer-sphere coupling or add directly to photocatalytically generated (bpy)Ni^I(Br) (**Int-2**) for inner-sphere coupling.[61] Upon adding to **Ni−B** to give **Int-1**, methyl radical can undergo outer-sphere coupling (i.e., S_H2) with a halide-derived alkyl radical generated via (bpy)Ni^I(X)-mediated XAT. In the case of inner-sphere coupling, the acetal-derived radical would add to **Int-2** to give (bpy)Ni^{II}(alkyl)(Br) (i.e., **Int-3**). Reduction of **Int-3** via Ir^{II}-catalyzed SET[62] would furnish a (bpy)Ni^I(alkyl) species (**Int-4**) poised for activating the alkyl halide via XAT. Following halide activation to form **Int-5**, C−C bond formation would occur via radical rebound onto Ni, followed by inner-sphere reductive elimination from the resulting Ni^{III} intermediate (**Int-6**) to forge the alkyl−alkyl coupled product and regenerate **Int-2**. On the basis of experimental evidence, methylation of alkyl halides benefits the most from the dual Ni catalyst system (i.e., **Ni−A** + **Ni−B**), with the nature of the halide dictating the extent to which outer- or inner-sphere coupling occurs. The α-chloro carbonyl derivatives appear to favor outer-sphere cross-coupling via cooperative XAT and S_H2, while alkyl bromides appear to benefit from cooperativity between this outer-sphere process and the inner-sphere coupling cycle. All other alkylations seem to predominantly favor inner-sphere coupling facilitated by reduced **Ni−A** (i.e., **Int-2**). Given the complex nature of this catalytic regime, there are instances where these Ni intermediates can go off-cycle. Under the standard photoredox conditions, **Int-3** may decompose to **Int-2** via photolysis of the Ni-alkyl bond (Figure 15B). In such a case, **Int-2** can quickly get back onto either the XAT cycle or the inner-sphere cycle and facilitate productive chemistry. Also of note is that if photolysis of **Int-3** does occur to produce a free methyl radical, this radical can be captured by **Ni−B** for productive S_H2 coupling, thus mitigating any deleterious effects on desired C−C bond formation.

CONCLUSION

In summary, we have developed a general strategy for cross-coupling methyl radical, derived from commercially available benzaldehyde dimethyl acetal, to electronically and structurally diverse alkyl chlorides and bromides by merging a unique cooperative dual Ni catalytic platform with photoredox catalysis. While a single Ni catalyst approach was initially sufficient for affording moderate yields of product, early mechanistic insight suggested that cooperativity between XAT, S_H2, and inner-sphere coupling cycles may be operative, thus guiding the strategic development of a dual Ni catalyst approach tailored to enhancing alkyl halide methylation. The synthetic utility of this Ni/photoredox platform was further demonstrated by modifying the acetal coupling partner such that a diverse array of alkyl radicals could be coupled to both primary and secondary alkyl bromides. A combination of experimental and computational mechanistic studies provided support for our initial hypothesis of C−C bond formation occurring by both outer-sphere and inner-sphere coupling. Specifically, inner-sphere coupling was found to occur at a (bpy)Ni^I(Br) catalyst via a sequence of elementary steps involving radical capture, reduction, XAT/radical rebound, and Ni^{III} reductive elimination, while outer-sphere coupling is proposed to occur via (bpy)Ni^I(Br)-mediated XAT of an alkyl halide, followed by (Tp*)Ni^{II}(acac)-catalyzed S_H2. Additionally, preparation and evaluation of a catalytically relevant (bpy)Ni^{II}(alkyl)(Br) complex provided valuable insight into additional mechanistic scenarios, including potential off-cycle reactivity. These studies ultimately shed light on how different substrate combinations can influence the preferred route for C−C bond formation. Overall, this work not only establishes a synthetically valuable approach to alkylating various C(sp^3)−halides but also provides fundamental mechanistic insights that future practitioners can draw upon when navigating the complex landscape of Ni/photoredox-catalyzed alkyl−alkyl cross-coupling.

ASSOCIATED CONTENT

Supporting Information

The Supporting Information is available free of charge at https://pubs.acs.org/doi/10.1021/jacs.5c10906.

Experimental procedures, characterization data, NMR spectra, and X-ray crystallographic data (PDF) (PDF)

Accession Codes

Accession Codes Crystallographic data for the structure reported in this article has been deposited at the Cambridge Crystallographic Data Centre (CCDC) under deposition number CCDC 2373324 (**Ni−C•**pentane). This data can be obtained free of charge from https://www.ccdc.cam.ac.uk/structures/. Experimental details and characterization data are provided in the Supporting Information.

AUTHOR INFORMATION

Corresponding Authors

Matthew J. Bird − *Chemistry Division, Brookhaven National Laboratory, Upton, New York 11973, United States;* orcid.org/0000-0002-6819-5380; Email: mbird@bnl.gov

Osvaldo Gutierrez − *Department of Chemistry and Biochemistry, University of California Los Angeles, Los Angeles, California 90095, United States;* orcid.org/0000-0001-8151-7519; Email: o.gutierrez@g.ucla.edu

Abigail G. Doyle − *Department of Chemistry and Biochemistry, University of California Los Angeles, Los Angeles, California 90095, United States;* orcid.org/0000-0002-6641-0833; Email: abigailgdoyle@g.ucla.edu

Authors

Erin M. Bucci − *Department of Chemistry and Biochemistry, University of California Los Angeles, Los Angeles, California 90095, United States;* orcid.org/0009-0006-2335-9819

Melecio A. Perea − *Department of Chemistry and Biochemistry, University of California Los Angeles, Los Angeles, California 90095, United States*

Remy F. Lalisse − *Department of Chemistry and Biochemistry, University of California Los Angeles, Los Angeles, California 90095, United States*

Poulami Mukherjee − *Department of Chemistry and Biochemistry, University of California Los Angeles, Los*

https://doi.org/10.1021/jacs.5c10906
J. Am. Chem. Soc. XXXX, XXX, XXX−XXX

Angeles, California 90095, United States; orcid.org/0000-0002-2876-7612

T. Judah Raab − *Department of Chemistry and Biochemistry, University of California Los Angeles, Los Angeles, California 90095, United States;* orcid.org/0000-0001-9449-5574

Lakshmy Kannadi Valloli − *Chemistry Division, Brookhaven National Laboratory, Upton, New York 11973, United States;* orcid.org/0000-0003-1836-5916

Daniel S. Min − *Department of Chemistry and Biochemistry, University of California Los Angeles, Los Angeles, California 90095, United States*

Complete contact information is available at: https://pubs.acs.org/10.1021/jacs.5c10906

Author Contributions

[§]E.M.B and M.A.P. contributed equally and are listed in alphabetical order.

Notes

The authors declare no competing financial interest.

■ ACKNOWLEDGMENTS

A.G.D. acknowledges NIH NIGMS (R35GM126986) for financial support. O.G. acknowledges NIH NIGMS (R35GM137797) for funding and Texas A&M University HPRC resources (https://hprc.tamu.edu) and the Hoffman2Cluster at UCLA Office of Advanced Research Computing's Research Technology Group for computational resources. The pulse radiolysis studies (M.J.B. and L.K.V.) were supported by BioLEC (Bioinspired Light-Escalated Chemistry), an Energy Frontier Research Center funded by the U.S. Department of Energy, Office of Science, Basic Energy Sciences, under Award no. DESC0019370. Use of the Laser Electron Accelerator Facility (LEAF) of the BNL Accelerator Center for Energy Research (ACER) was supported by U.S. Department of Energy, Office of Science, Office of Basic Energy Sciences, Division of Chemical Sciences, Geosciences & Bioscience through contract DE-SC0012704. This material is based upon work supported by the National Science Foundation MPS-Ascend Postdoctoral Research Fellowship (for M.A.P.) under grant no. 2213210. Additional support for this research was provided by shared instrumentation grant no. rese and the NIH Office of Research Infrastructure Programs under grant no. S10OD028644. We thank Shutian Jiang for help with data science-guided construction of the alkyl bromide scope and Flora Fan for synthesis of boc-protected celecoxib.

■ REFERENCES

(1) Lovering, F.; Bikker, J.; Humblet, C. Escape from Flatland: Increasing Saturation as an Approach to Improving Clinical Success. *J. Med. Chem.* **2009**, *52*, 6752−6756.

(2) Lovering, F. Escape from Flatland 2: Complexity and Promiscuity. *MedChemComm* **2013**, *4*, 515−519.

(3) Buskes, M. J.; Blanco, M.-J. Impact of Cross-Coupling Reactions in Drug Discovery and Development. *Molecules* **2020**, *25*, 3493.

(4) Poremba, K. E.; Dibrell, S. E.; Reisman, S. E. Nickel-Catalyzed Enantioselective Reductive Cross-Coupling Reactions. *ACS Catal.* **2020**, *10*, 8237−8246.

(5) Richmond, E.; Moran, J. Recent Advances in Nickel Catalysis Enabled by Stoichiometric Metallic Reducing Agents. *Synthesis* **2018**, *50*, 499−513.

(6) Chan, A. Y.; Perry, I. B.; Bissonnette, N. B.; Buksh, B. F.; Edwards, G. A.; Frye, L. I.; Garry, O. L.; Lavagnino, M. N.; Li, B. X.; Liang, Y.; Mao, E.; Millet, A.; Oakley, J. V.; Reed, N. L.; Sakai, H. A.; Seath, C. P.; MacMillan, D. W. C. Metallaphotoredox: The Merger of Photoredox and Transition Metal Catalysis. *Chem. Rev.* **2022**, *122*, 1485−1542.

(7) Jose, J.; Diana, E. J.; Kanchana, U. S.; Mathew, T. V. Recent Advances in the Nickel-catalysed Electrochemical Coupling Reactions with a Focus on the Type of Bond Formed. *Asian J. Org. Chem.* **2023**, *12*, No. e202200593.

(8) Franke, M. C.; Weix, D. J. Recent Advances in Electrochemical, Ni-Catalyzed C−C Bond Formation. *Isr. J. Chem.* **2024**, *64*, No. e202300089.

(9) Arendt, K. M.; Doyle, A. G. Dialkyl Ether Formation by Nickel-Catalyzed Cross-Coupling of Acetals and Aryl Iodides. *Angew. Chem., Int. Ed.* **2015**, *54*, 9876−9880.

(10) Dongbang, S.; Doyle, A. G. Ni/Photoredox-Catalyzed C(sp3)−C(sp^3) Coupling between Aziridines and Acetals as Alcohol-Derived Alkyl Radical Precursors. *J. Am. Chem. Soc.* **2022**, *144*, 20067−20077.

(11) Graham, T. J. A.; Doyle, A. G. Nickel-Catalyzed Cross-Coupling of Chromene Acetals and Boronic Acids. *Org. Lett.* **2012**, *14*, 1616−1619.

(12) Kariofillis, S. K.; Jiang, S.; Żurański, A. M.; Gandhi, S. S.; Martinez Alvarado, J. I.; Doyle, A. G. Using Data Science to Guide Aryl Bromide Substrate Scope Analysis in a Ni/Photoredox-Catalyzed Cross-Coupling with Acetals as Alcohol-Derived Radical Sources. *J. Am. Chem. Soc.* **2022**, *144*, 1045−1055.

(13) Kariofillis, S. K.; Shields, B. J.; Tekle-Smith, M. A.; Zacuto, M. J.; Doyle, A. G. Nickel/Photoredox-Catalyzed Methylation of (Hetero)Aryl Chlorides Using Trimethyl Orthoformate as a Methyl Radical Source. *J. Am. Chem. Soc.* **2020**, *142*, 7683−7689.

(14) Huang, C.-Y.; Doyle, A. G. Nickel-Catalyzed Negishi Alkylations of Styrenyl Aziridines. *J. Am. Chem. Soc.* **2012**, *134*, 9541−9544.

(15) Nielsen, D. K.; Huang, C.-Y.; Doyle, A. G. Directed Nickel-Catalyzed Negishi Cross Coupling of Alkyl Aziridines. *J. Am. Chem. Soc.* **2013**, *135*, 13605−13609.

(16) Steiman, T. J.; Liu, J.; Mengiste, A.; Doyle, A. G. Synthesis of *β*-Phenethylamines via Ni/Photoredox Cross-Electrophile Coupling of Aliphatic Aziridines and Aryl Iodides. *J. Am. Chem. Soc.* **2020**, *142*, 7598−7605.

(17) Williams, W. L.; Gutiérrez-Valencia, N. E.; Doyle, A. G. Branched-Selective Cross-Electrophile Coupling of 2-Alkyl Aziridines and (Hetero)Aryl Iodides Using Ti/Ni Catalysis. *J. Am. Chem. Soc.* **2023**, *145*, 24175−24183.

(18) Nielsen, D. K.; Doyle, A. G. Nickel-Catalyzed Cross-Coupling of Styrenyl Epoxides with Boronic Acids. *Angew. Chem., Int. Ed.* **2011**, *50*, 6056−6059.

(19) Parasram, M.; Shields, B. J.; Ahmad, O.; Knauber, T.; Doyle, A. G. Regioselective Cross-Electrophile Coupling of Epoxides and (Hetero)Aryl Iodides via Ni/Ti/Photoredox Catalysis. *ACS Catal.* **2020**, *10*, 5821−5827.

(20) Lau, S. H.; Borden, M. A.; Steiman, T. J.; Wang, L. S.; Parasram, M.; Doyle, A. G. Ni/Photoredox-Catalyzed Enantioselective Cross-Electrophile Coupling of Styrene Oxides with Aryl Iodides. *J. Am. Chem. Soc.* **2021**, *143*, 15873−15881.

(21) Cagan, D. A.; Bím, D.; Kazmierczak, N. P.; Hadt, R. G. Mechanisms of Photoredox Catalysis Featuring Nickel−Bipyridine Complexes. *ACS Catal.* **2024**, *14*, 9055−9076.

(22) Cagan, D. A.; Bím, D.; McNicholas, B. J.; Kazmierczak, N. P.; Oyala, P. H.; Hadt, R. G. Photogenerated Ni(I)−Bipyridine Halide Complexes: Structure−Function Relationships for Competitive C-(sp^2)−Cl Oxidative Addition and Dimerization Reactivity Pathways. *Inorg. Chem.* **2023**, *62*, 9538−9551.

(23) Ting, S. I.; Williams, W. L.; Doyle, A. G. Oxidative Addition of Aryl Halides to a Ni(I)-Bipyridine Complex. *J. Am. Chem. Soc.* **2022**, *144*, 5575−5582.

(24) Newman-Stonebraker, S. H.; Raab, T. J.; Roshandel, H.; Doyle, A. G. Synthesis of Nickel(I)−Bromide Complexes via Oxidation and Ligand Displacement: Evaluation of Ligand Effects on Speciation and Reactivity. *J. Am. Chem. Soc.* **2023**, *145*, 19368−19377.

(25) Gutierrez, O.; Tellis, J. C.; Primer, D. N.; Molander, G. A.; Kozlowski, M. C. Nickel-Catalyzed Cross-Coupling of Photoredox-Generated Radicals: Uncovering a General Manifold for Stereoconvergence in Nickel-Catalyzed Cross-Couplings. *J. Am. Chem. Soc.* **2015**, *137*, 4896−4899.
(26) Shu, W.; García-Domínguez, A.; Quirós, M. T.; Mondal, R.; Cárdenas, D. J.; Nevado, C. Ni-Catalyzed Reductive Dicarbofunctionalization of Nonactivated Alkenes: Scope and Mechanistic Insights. *J. Am. Chem. Soc.* **2019**, *141*, 13812.
(27) Lin, Q.; Spielvogel, E. H.; Diao, T. Carbon-Centered Radical Capture at Nickel(II) Complexes: Spectroscopic Evidence, Rates, and Selectivity. *Chem.* **2023**, *9*, 1295−1308.
(28) Yuan, M.; Song, Z.; Badir, S. O.; Molander, G. A.; Gutierrez, O. On the Nature of $C(sp^3)$−$C(sp^2)$ Bond Formation in Nickel-Catalyzed Tertiary Radical Cross-Couplings: A Case Study of Ni/Photoredox Catalytic Cross-Coupling of Alkyl Radicals and Aryl Halides. *J. Am. Chem. Soc.* **2020**, *142*, 7225−7234.
(29) Wang, L.; Zhou, P.-P.; Xie, D.; Yue, Q.; Sun, H.-Z.; Yang, S.-D.; Wang, G.-W. Dynamic Kinetic Activation of Aziridines Enables Radical-Polar Crossover (4 + 3) Cycloaddition with 1,3-Dienes. *J. Am. Chem. Soc.* **2025**, *147*, 2675−2688.
(30) Biswas, S.; Weix, D. J. Mechanism and Selectivity in Nickel-Catalyzed Cross-Electrophile Coupling of Aryl Halides with Alkyl Halides. *J. Am. Chem. Soc.* **2013**, *135*, 16192−16197.
(31) Lin, Q.; Fu, Y.; Liu, P.; Diao, T. Monovalent Nickel-Mediated Radical Formation: A Concerted Halogen-Atom Dissociation Pathway Determined by Electroanalytical Studies. *J. Am. Chem. Soc.* **2021**, *143*, 14196−14206.
(32) Tsymbal, A. V.; Bizzini, L. D.; MacMillan, D. W. C. Nickel Catalysis via S_H2 Homolytic Substitution: The Double Decarboxylative Cross-Coupling of Aliphatic Acids. *J. Am. Chem. Soc.* **2022**, *144*, 21278−21286.
(33) Mao, E.; MacMillan, D. W. C. Late-Stage $C(sp^3)$−H Methylation of Drug Molecules. *J. Am. Chem. Soc.* **2023**, *145*, 2787−2793.
(34) Sakai, H. A.; MacMillan, D. W. C. Nontraditional Fragment Couplings of Alcohols and Carboxylic Acids: $C(sp^3)$−$C(sp^3)$ Cross-Coupling via Radical Sorting. *J. Am. Chem. Soc.* **2022**, *144*, 6185−6192.
(35) Everson, D. A.; Shrestha, R.; Weix, D. J. Nickel-Catalyzed Reductive Cross-Coupling of Aryl Halides with Alkyl Halides. *J. Am. Chem. Soc.* **2010**, *132*, 920−921.
(36) Hamby, T. B.; LaLama, M. J.; Sevov, C. S. Controlling Ni Redox States by Dynamic Ligand Exchange for Electroreductive $C(sp^3)$−$C(sp^2)$ Coupling. *Science* **2022**, *376*, 410−416.
(37) Hernández-Mejías, A. D.; Shimozono, A. M.; Hazra, A.; Richter, S.; Tong, Z.; Langille, N. F.; Quasdorf, K.; Parsons, A. T.; Sigman, M. S.; Reisman, S. E. Ni-Catalyzed Enantioselective Desymmetrization: Development of Divergent Acyl and Decarbonylative Cross-Coupling Reactions. *J. Am. Chem. Soc.* **2025**, *147*, 3468−3477.
(38) Cusumano, A. Q.; Chaffin, B. C.; Doyle, A. G. Mechanism of Ni-Catalyzed Photochemical Halogen Atom-Mediated $C(sp^3)$−H Arylation. *J. Am. Chem. Soc.* **2024**, *146*, 15331−15344.
(39) Akana, M. E.; Tcyrulnikov, S.; Akana-Schneider, B. D.; Reyes, G. P.; Monfette, S.; Sigman, M. S.; Hansen, E. C.; Weix, D. J. Computational Methods Enable the Prediction of Improved Catalysts for Nickel-Catalyzed Cross-Electrophile Coupling. *J. Am. Chem. Soc.* **2024**, *146*, 3043−3051.
(40) Duan, L.; Lin, Y.; An, Q.; Zuo, Z. Synergistic LMCT and Ni Catalysis for Methylative Cross-Coupling Using Tert-Butanol: Modulating Radical Pathways via Selective Bond Homolysis. *J. Am. Chem. Soc.* **2025**, *147*, 14785−14796.
(41) Ruos, M. E.; Kinney, R. G.; Ring, O. T.; Doyle, A. G. A General Photocatalytic Strategy for Nucleophilic Amination of Primary and Secondary Benzylic C−H Bonds. *J. Am. Chem. Soc.* **2023**, *145*, 18487−18496.
(42) Lovett, G. H.; Chen, S.; Xue, X.-S.; Houk, K. N.; MacMillan, D. W. C. Open-Shell Fluorination of Alkyl Bromides: Unexpected Selectivity in a Silyl Radical-Mediated Chain Process. *J. Am. Chem. Soc.* **2019**, *141*, 20031−20036.
(43) Smith, R. T.; Zhang, X.; Rincón, J. A.; Agejas, J.; Mateos, C.; Barberis, M.; García-Cerrada, S.; de Frutos, O.; MacMillan, D. W. C. Metallaphotoredox-Catalyzed Cross-Electrophile $C(sp^3)$−$C(sp^3)$ Coupling of Aliphatic Bromides. *J. Am. Chem. Soc.* **2018**, *140*, 17433−17438.
(44) Lin, P. C.; Wong, C. D.; Jarvo, E. R. Cross-selective Deoxygenative Coupling of Aliphatic Alcohols: Installation of Methyl Groups Including Isotopic Labels by Nickel Catalysis. *Angew. Chem., Int. Ed.* **2024**, *63*, No. e202403119.
(45) Till, N. A.; Oh, S.; MacMillan, D. W. C.; Bird, M. J. The Application of Pulse Radiolysis to the Study of Ni(I) Intermediates in Ni-Catalyzed Cross-Coupling Reactions. *J. Am. Chem. Soc.* **2021**, *143*, 9332−9337.
(46) Wishart, J. F.; Cook, A. R.; Miller, J. R. The LEAF Picosecond Pulse Radiolysis Facility at Brookhaven National Laboratory. *Rev. Sci. Instrum.* **2004**, *75*, 4359−4366.
(47) DiLuzio, S.; Kannadi Valloli, L.; Kudisch, M.; Chambers, D. T.; Rumbles, G.; Reid, O. G.; Bird, M. J.; Sayre, H. J. Reconceptualizing the Ir^{III} Role in Metallaphotoredox Catalysis: From Strong Photooxidant to Potent Energy Donor. *ACS Catal.* **2024**, *14*, 11378−11388.
(48) Turro, R. F.; Wahlman, J. L. H.; Tong, Z. J.; Chen, X.; Yang, M.; Chen, E. P.; Hong, X.; Hadt, R. G.; Houk, K. N.; Yang, Y.-F.; Reisman, S. E. Mechanistic Investigation of Ni-Catalyzed Reductive Cross-Coupling of Alkenyl and Benzyl Electrophiles. *J. Am. Chem. Soc.* **2023**, *145*, 14705−14715.
(49) Anghileri, L.; Baunis, H.; Bena, A. R.; Giannoudis, C.; Burke, J. H.; Reischauer, S.; Merschjann, C.; Wallick, R. F.; Al Said, T.; Adams, C. E.; Simionato, G.; Kovalenko, S.; Dell'Amico, L.; van der Veen, R. M.; Pieber, B. Evidence for a Unifying Ni^{I}/Ni^{III} Mechanism in Light-Mediated Cross-Coupling Catalysis. *J. Am. Chem. Soc.* **2025**, *147*, 13169−13179.
(50) Li, J.; Kang, T.; Xiao, Y.; Li, Z.; Xiao, Y.; Yan, Y.; Song, G.; Li, G.; Dong, J.; Wang, C.; Xue, D. The Multiple Roles of Bipyridine-Nickel(II) Complex in Versatile Photoredox $C(sp^2)$−$C(sp^3)$ Cross-Coupling. *ACS Catal.* **2025**, *15*, 3328−3338.
(51) Raab, T. J.; Doyle, A. G. Reactivity Studies of Bipyridine-Ligated Ni(I) and Ni(0) Complexes Inform the Mechanism in Modern Cross-Coupling Reactions. *J. Am. Chem. Soc.* **2025**, *147*, 33991−34000.
(52) Isolation and characterization of the analogous (dtbbpy)Ni^{II}(Me)(Br) complex (**Ni-C**, *vide infra*) revealed a ground state singlet species with a low adiabatic singlet−triplet gap, indicating that DFT computations may be slightly overestimating the stability of ^{3}Int-3. However, given the small difference in energy between ^{1}Int-3 and ^{3}Int-3, this overestimation does not conflict with the mechanistic proposal.
(53) Zhang, L.; Wang, H.; Santiago, T. G.; Yue, W.-J.; Martin, R. Photoinduced Nickel-Catalysed Enantioconvergent sp^3−sp^3 Coupling of Unactivated Olefins and Aziridines. *Nat. Catal.* **2025**, *8*, 348−356.
(54) Yamaguchi, Y.; Ichioka, H.; Klein, A.; Brennessel, W. W.; Vicic, D. A. Linear Bis(Perfluoroalkyl) Complexes of Nickel Bipyridine. *Organometallics* **2012**, *31*, 1477−1483.
(55) Zhang, Y.; Tanabe, Y.; Kuriyama, S.; Nishibayashi, Y. Photoredox- and Nickel-Catalyzed Hydroalkylation of Alkynes with 4-Alkyl-1,4-dihydropyridines: Ligand-Controlled Regioselectivity. *Chem.−Eur. J.* **2022**, *28*, No. e202200727.
(56) Ting, S. I.; Garakyaraghi, S.; Taliaferro, C. M.; Shields, B. J.; Scholes, G. D.; Castellano, F. N.; Doyle, A. G. 3d-d Excited States of Ni(II) Complexes Relevant to Photoredox Catalysis: Spectroscopic Identification and Mechanistic Implications. *J. Am. Chem. Soc.* **2020**, *142*, 5800−5810.
(57) Shields, B. J.; Kudisch, B.; Scholes, G. D.; Doyle, A. G. Long-Lived Charge-Transfer States of Nickel(II) Aryl Halide Complexes Facilitate Bimolecular Photoinduced Electron Transfer. *J. Am. Chem. Soc.* **2018**, *140*, 3035−3039.

https://doi.org/10.1021/jacs.5c10906
J. Am. Chem. Soc. XXXX, XXX, XXX−XXX

(58) Westawker, L. P.; Bouley, B. S.; Vura-Weis, J.; Mirica, L. M. Photochemistry of Ni(II) Tolyl Chlorides Supported by Bidentate Ligand Frameworks. *J. Am. Chem. Soc.* **2025**, *147*, 17315−17329.
(59) Wang, C.; Dong, G. Direct β-Alkylation of Ketones and Aldehydes via Pd-Catalyzed Redox Cascade. *J. Am. Chem. Soc.* **2018**, *140*, 6057−6061.
(60) Zhang, P.; Le, C.; MacMillan, D. W. C. Silyl Radical Activation of Alkyl Halides in Metallaphotoredox Catalysis: A Unique Pathway for Cross-Electrophile Coupling. *J. Am. Chem. Soc.* **2016**, *138*, 8084−8087.
(61) The reversibility of this radical addition is supported by DFT-level calculations (see Supporting Information Section 8, Figure S43 for details).
(62) In accord with Stern−Vomer emission quenching studies performed in ref 12 with the analogous (dtbbpy)Ni^{II}(o-Tol)(Br) complex and TBABr, it is expected that excited-state photocatalyst quenching by LiBr would be kinetically competitive with excited-state photocatalyst quenching by **Int-3**, thus endering reduction of **Int-3** to **Int-2** to occur via an SET pathway from Ir^{II}.

https://doi.org/10.1021/jacs.5c10906
J. Am. Chem. Soc. XXXX, XXX, XXX−XXX